

Modeling and Force Estimation of Cardiac Catheters for Haptics-enabled Tele-intervention

Amir Sayadi

A Thesis
in
Mechanical, Industrial, Aerospace Engineering

Presented in Partial Fulfillment of the Requirements
For the Degree of
Master of Applied Science (Mechanical Engineering) at
Concordia University
Montréal, Québec, Canada

October 2021

© Amir Sayadi, 2021

CONCORDIA UNIVERSITY
School of Graduate Studies

This is to certify that the thesis prepared

By: **Amir Sayadi**

Entitled: **Modeling and Force Estimation of Cardiac Catheters for Haptics-enabled Tele-intervention**

and submitted in partial fulfillment of the requirements for the degree of

Master of Applied Science (Mechanical Engineering)

complies with the regulations of this University and meets the accepted standards with respect to originality and quality.

Signed by the final examining committee:

_____ Chair
Dr. Subhash Rakheja

_____ External
Dr. Shahin Hashtrudi Zad

_____ Examiner
Dr. Subhash Rakheja

_____ Examiner

_____ Thesis Supervisor
Dr. Javad Dargahi

Approved by _____
Dr. Martin Pugh, Chair of Department

Oct. 20, 2021 _____
Dr. Mourad Debbabi, Dean
Gina Cody School of Engineering and Computer Science

Abstract

Modeling and Force Estimation of Cardiac Catheters for Haptics-enabled Tele-intervention

Amir Sayadi

Robot-assisted cardiovascular intervention (RCI) systems have shown success in reducing the x-ray exposure to surgeons and patients during cardiovascular interventional procedures. RCI systems typically are teleoperated systems with leader-follower architecture. With such system architecture the surgeon is placed out of x-ray exposure zone and uses a console to control the robot remotely. Despite its success in reducing x-ray exposure, clinicians have identified the lack of force feedback as its main technological limitation that can lead to vascular perforation of the patient's vessels and even their death. The objective of this thesis was to develop, verify, and validate mechatronics technology for real-time accurate and robust haptic feedback rendering for RCI systems. To attain the thesis objective, first, a thorough review of the state-of-the-art clinical requirements, modeling approaches and methods, and current knowledge gaps for the provision of force feedback for RCI systems was performed. Afterward, a real-time tip force estimation method based on image-based shape-sensing and learning-from-simulation was developed and validated. The learning-based model was fairly accurate but required a large database for training which was computationally expensive. Next, a new mechanistic model, i.e., finite arc method (FAM) for soft robots was proposed, formulated, solved, and validated that allowed for fast and accurate modeling of catheter deformation. With FAM, the required training database for the proposed learning-from-simulation method would be generated with high speed and accuracy. In the end, to robustly relay the estimated forces from real-time imaging from the follower robot to the leader haptic device, a novel impedance-based force feedback rendering modality was proposed and implemented on a representative teleoperated RCI system for experimental validation. The proposed method was compared with the classical direct force reflection method and showed enhanced stability, robustness, and accuracy in the presence of communication disruption. The results of this thesis showed that the performance of the proposed integrated force feedback rendering system was in fair compliance with the clinical requirements and had superior robustness compared to the classical direct force reflection method.

Acknowledgments

This thesis provided me with a unique and unforgettable life experience. It not only enhanced my education but also provided me the opportunity to meet a lot of new people and learn about the culture of different nations. Thanks to the God, the Almighty, for His showers of blessings throughout my research work to complete the research successfully. I am extremely grateful to my parents, Farideh and Mohammad, for their love, prayers, caring, and sacrifices for educating and preparing me for my future. Also, I express my thanks to my sister and brother, Sadaf and Ali, for their support and valuable prayers.

I would like to express my deep and sincere gratitude to my research supervisor, Dr. Javad Dargahi, for giving me this opportunity to research and providing the facilities needed throughout this research. I am extending my heartfelt thanks to him for his acceptance and patience during the discussion I had with him on research work and thesis preparation.

I am extending my thanks to Dr. Amir Hooshidar for all he has done and, in particular, his support during this research. His dynamism, vision, sincerity, and motivation have deeply inspired me. He has taught me the methodology to carry out the research and to present the research works as clearly as possible. I would like to say thanks to my colleagues and my friends, especially Nima, for their constant encouragement. I would also like to thank them for their friendship, empathy, inspiration, and everything I have learned from them. A sincere thank you to Dr. Shahram Shokouhfar for his genuine support throughout my academic life. It was a great privilege and honor to work and study under his guidance. I am extremely grateful for what he has offered me.

My special thanks go to my friend Bahar, who has always motivated me to live the way I love and move towards what I desire.

Thank you amazing staff of Concordia University. As it would be impossible to thank everyone individually, please accept this acknowledgment as an expression of my deepest gratitude.

Amir Sayadi

Contents

List of Figures	viii
List of Tables	xi
Nomenclatures	xii
1 Introduction	1
1.1 Background	1
1.1.1 Cardiovascular Diseases	1
1.1.2 Treatment Approaches	3
1.1.3 Robot-assisted Cardiovascular Intervention	4
1.1.4 Clinical Need for Force Feedback	5
1.2 Literature Review	7
1.2.1 Modeling a catheter as a soft robot	7
1.2.2 Geometric models	9
1.2.3 Force Feedback Rendering for RCI	10
1.2.4 Force Estimation: Haptic Cue	12
1.3 Problem Definition	16
1.4 Research Objectives	17
1.5 Research Scope	17
1.6 Contributions	18

1.7	Thesis Layout	19
2	Tip Force Estimation on Soft Flexural Robots through Shape-sensing and Simulation-based Training with <i>ex-vivo</i> Validation	22
2.1	Introduction	23
2.1.1	Background	23
2.1.2	Objective and Contributions	25
2.2	Simulation and Shape Sensing	26
2.2.1	Finite Element Simulation and Verification	26
2.2.2	Shape Sensing	28
2.3	Learning-based Force Estimation	31
2.3.1	Dataset	31
2.3.2	Model Selection and Training	32
2.4	<i>ex-vivo</i> Validation Study	34
2.5	Summary	37
3	Mechanical Modeling of Soft Tendon-Driven Robots with Large Deformation: Finite Arc Method (FAM)	38
3.1	Introduction	39
3.1.1	Background	39
3.1.2	Related Studies	40
3.1.3	Contributions	42
3.2	Material and Methods	42
3.2.1	Kinematics	42
3.2.2	Constitutive Equation	45
3.2.3	Moment Balance	45
3.2.4	Deformation Solution	47

3.3	Validation Studies	50
3.3.1	Study I: Simulation-based Validation	50
3.3.2	Study II: Experimental Validation	54
3.4	Summary	57
4	Impedance Matching Approach for Robust Force Feedback Rendering with Application in Robot-assisted Interventions	58
4.1	Background	59
4.2	Material and Method	61
4.2.1	Proposed Force Feedback Framework	61
4.2.2	Impedance Estimation at Slave Module	63
4.2.3	Estimation of Force Feedback at Master Module	65
4.2.4	Comparison of PID Controller with IMA Controller	65
4.3	Validation Studies	66
4.3.1	Experiment I: Impedance Estimation at Slave Module	68
4.3.2	Experiment II: Comparison of DFR and IMA with Communication Interruption	70
4.4	Summary	72
5	Conclusions and Future Works	73
5.1	Conclusions	73
5.2	Future Works	75
	Bibliography	76

List of Figures

1	Conducting system or electrical system of the heart showing the specialised tissue that stimulates contraction	2
2	Ablation treatment with ablation catheter and mapping catheter. To access the ablation target areas, RFA catheter is passed through the atrial septum.	4
3	robot-assisted cardiovascular intervention	6
4	model-based haptic feedback approaches	13
5	Catheter ablation for atrial fibrillation	23
6	(a) Blazer II-XP under three-point-bending (3PB) test, (b) deformed shape of the catheter under axial loads.	25
7	Comparison of force-displacement curve between the FE simulation and experiment.	27
8	(a) Representative shape of the deflected catheter and its corresponding Bezier curve, (b) Bezier shape fitting and Bezier control points for a representative set of catheter deformations.	30
9	(a) Schematic architecture of ANN model for force estimation, (b) error of force estimation on test dataset for the trained ANN and SVR models.	33
10	(a) <i>ex-vivo</i> validation test setup, (b) binary segmented shape of the catheter during <i>ex-vivo</i> test, and (c) comparison of the estimated force with ANN and SVR models with the ground truth recorded by the UTM.	35

11	Distribution of force estimation error for ANN and SVR models in the <i>ex-vivo</i> test.	36
12	The schematic shape of steerable ablation catheters in the left atrium during ablation interventions.	40
13	Schematic deformed shape of the tendon-driven continuum arm Bezier spline centerline.	43
14	The free-body diagram (FBD) of a deformed catheter with multiple circular arc segments.	46
15	Eight load cases on a representative flexure for Study I.	50
16	Comparison of FAM and FEM results in deflection estimations for eight load cases on soft flexures.	51
17	Distribution of error of deformation estimation with FEM as the reference along (a) x-direction and (b) y-direction.	52
18	Effect of segmentation, (a) FAM deflection solution for different number of segments and (b) absolute tip displacement error for different number of segments.	53
19	Setup used in validation study-II (a) patient module, (b) deflected catheter in the vascular model with the external forces.	55
20	Comparison of FAM and ground truth deflections in Study II.	56
21	RCI system representation with DFR approach used for remote RCI procedures.	60
22	The proposed RCI system for remote RCI procedures with IMA-based force feedback.	62
23	RCI device used in the experiments: (a) master, (b) slave module.	67
24	(a) Inserted length and velocity of the catheter in Experiment I, (b) tracking performance of IMA, and (c) distribution of force tracking error.	69

25 (a) Force tracking performance of PID-based DFR, (b) force tracking performance of IMA controller, (c) temporal changes in impedance coefficients used by IMA, and (d) comparison of the force tracking error with PID-based DFR and IMA controller. 71

List of Tables

1 Comparison of FAM and FEM solutions for eight load cases. 51

Nomenclatures

Operators

\cdot	Dot product
\times	Cross product
$(\dot{\cdot})$	Spatial derivative operator with respect to t
$(\dot{\cdot})'$	Temporal derivative operator with respect to s

Greek Symbols

Γ	Bending plane
δt	Time increment
ν	Poisson's ratio
κ	Total curvature
κ_g	Geodesic curvature
λ	Curvature control parameter for Bezier shape interpolation
Π	Functional for deformation estimation
φ	Bending angle
Ψ	Camera calibration matrix

English Symbols

\mathbf{c}	Centerline of deformed B-spline
E	Elastic modulus
\mathbf{f}^{Tip}	Tip force vector
I	Second moment of inertia
$k_{P,I,D}$	Coefficients of PID controller
\mathbf{m}^{Tip}	Tip moment vector
\mathbf{p}	Control points of B-spline
r	Radius of curvature
\mathbf{R}	Rotation matrix
s	Normalized curve parameter
t	Time
u	Horizontal position of pixels in image
v	Vertical position of pixels in image
x	x-component of the tip position of catheter
y	y-component of the tip position of catheter
z	z-component of the tip position of catheter

Chapter 1

Introduction

1.1 Background

1.1.1 Cardiovascular Diseases

All around the world, cardiac problems are the leading cause of hospitalization and mortality. Coronary artery stenosis (CAS) is one of the most common cardiac disorders. Cardiology's other major clinical issue is arrhythmia, a disturbance of the heart rhythm and its conduction system [1, 2]. Figure 1 depicts the many components of the human heart's conduction system. With a prevalence rate of 0.95 percent, atrial fibrillation is the most frequent arrhythmia [3]. It is associated with a significant number of hospitalization and mortality from stroke, sudden cardiac death, heart failure [4]. Atrial fibrillation (AFib) or arrhythmia is mainly caused by an uneven discharge of signals from pulmonary veins (PVs) and will lead to serious heart-related complications. Cardiovascular diseases are the leading cause of death in the USA (39%) [5]. According to the American Heart Association, 2.7 million Americans have AFib, and according to current research, this number is expected to rise to 12.1 million by 2030 [6]. Electrocardiographic (ECG) analysis will provide a comprehensive picture of the patient's heart health. When heartbeats are not in

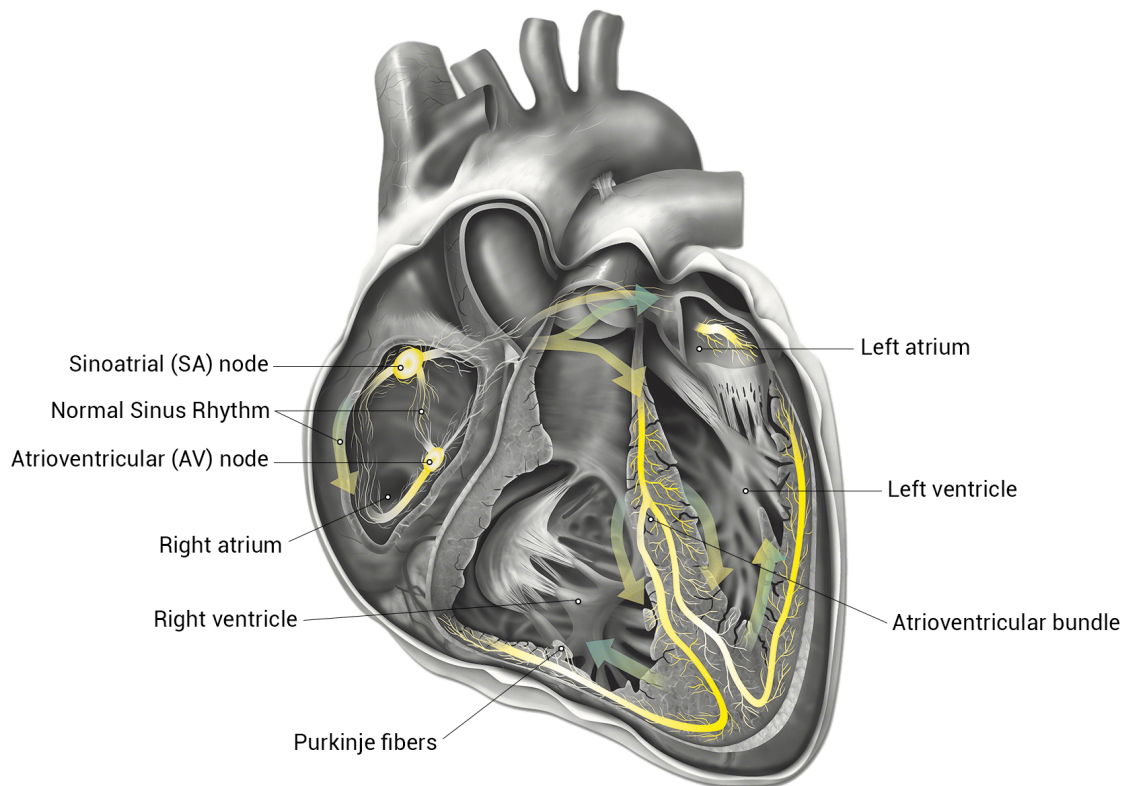


Figure 1: Conducting system or electrical system of the heart showing the specialised tissue that stimulates contraction. Contraction of the heart is usually initiated by the sinoatrial node (or SA node) and for this reason it is considered to be the heart's natural pacemaker.

sync, it has called cardiac arrhythmia. The pace of the beats is either quicker or slower than typical [7]. Some arithmetic heartbeats, such as ventricular fibrillation and tachycardia, pose a severe threat to the patient's life. Aberrant electrical characteristics of the heart produce arrhythmias, and sudden death can occur due to exercise or mental stress in some situations [8]. Atrial fibrillation is a frequent arrhythmia that affects people in their later years. Genetics and family history can also happen in a structurally normal heart, known as lone atrial fibrillation [9].

1.1.2 Treatment Approaches

In general, there are two types of arrhythmia therapies accessible today: medication therapy and non-drug therapy [10]. Antiarrhythmic drugs (AAD) have been the subject of several studies. Despite advances in technology, AADs are an effective medication therapy in treating ventricular arrhythmias [11]. Surgical ablation is a non-drug treatment for cardiac arrhythmias that has been replaced by several modalities of electromagnetic transcatheter ablation procedures. It is being hindered as a technique in which the muscles cause unwanted pulses or movement in the heart. Radiofrequency (RF) ablation is the most effective and widely used method. DC shock, laser, microwave, and ultrasound are some of the other modalities [12]. Although RFA-assisted pulmonary vein isolation is the most successful treatment for symptomatic patients, the success rate relies on the extent of the lesion and a thorough understanding of left atrial wall thickness (LAWT) [13]. The average human atrial wall thickness was observed to be roughly 2 mm [14]. M. Bishop developed a novel approach for measuring the (LAWT) in 2015 [15], which involved solving the Laplace equation over a finite element mesh of the left atrium obtained from a segmented computed tomographic angiography (CTA) dataset.

Radiofrequency ablation [16], a well-known and well-accepted therapy for problems such as arrhythmia, is performed using catheters inserted into the heart chamber. The use of steerable catheters in cardiology, neurology, and endovascular diagnosis and treatment is expected (see Fig 2). The treatment of arrhythmia is the most common application of steerable catheters [17]. The Real-Time Contact Force Curve has been shown to predict the size of a radiofrequency lesion, which is used to treat arrhythmias [18]. Dingfei et al.[19] suggested a Computer-assisted arrhythmia recognition system to detect and categorize arrhythmias. Moreover, the results demonstrated that autoregressive modeling (AR) was a feasible solution to cardiac arrhythmias with reasonable accuracies.

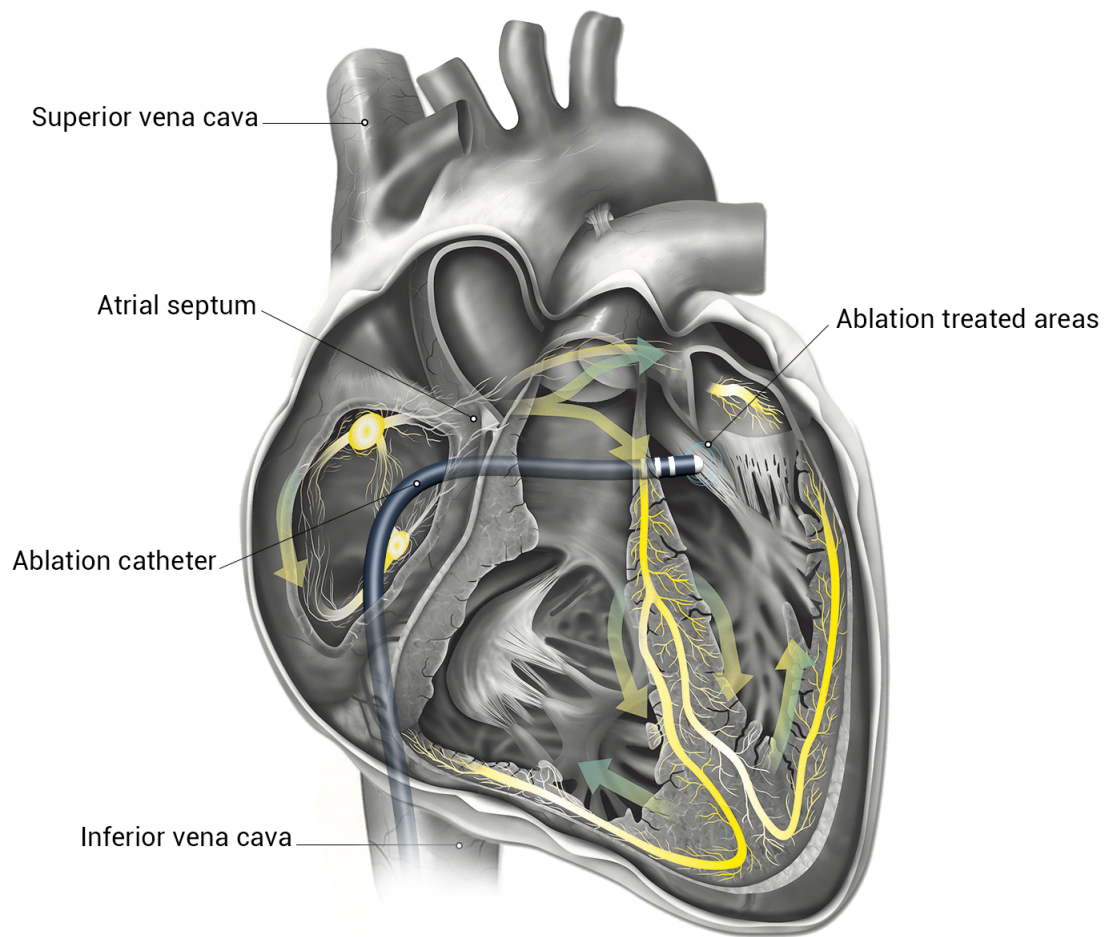


Figure 2: Ablation treatment with ablation catheter and mapping catheter. To access the ablation target areas, RFA catheter is passed through the atrial septum.

1.1.3 Robot-assisted Cardiovascular Intervention

Minimally invasive surgery is a type of surgery in which a tiny incision is made in the patient's body, and surgery is performed using something like a laparoscopic device through small diameter trocars inserted into the wound. The trocar is a sharp-edged medical and surgical device used to access to internal blood vessels and cavities. Minimally invasive surgery provides several advantages over open and regular operations, including a lower risk of patient damage, a faster recovery time, and cheaper healthcare expenditures. The

improvements described in minimally invasive surgery are often obtained through improving surgical instrument skill and agility and incorporating robot systems such as manipulators, control, and routing. In addition, by scaling the movement of the master and slave robots, the robot structure may reduce the surgeon's handshaking. The results of the robotic-assisted operations were described as positive and successful. In 2013, Giora. W et al. reported a success rate of 98.8% when using these novel ways to execute percutaneous coronary intervention (PCI) [20]. Compared to traditional techniques, enhanced PCI was found to be both safe and effective [21]. Aside from the benefits that new catheterization procedures provide, there are some drawbacks to this new approach. During Robotic-assisted procedures, loss of touch is a significant problem [22]. While the manipulator treats or diagnoses the patient, the haptic input between the manipulator's hands and the organ within the patient's body is lost and must be compensated. The manipulator controls the position by spinning the proximal section of the catheter outside the patient's body while obtaining natural input from his or her hand when doing manual catheterization. As depicted in Fig. 3, this configuration lowered X-ray exposure to the operator and staff while it imposed new health hazards on the patient, mainly due to haptic feedback loss throughout the process [22]. Furthermore, the vibration transmitted by a catheter with force at the tip of the catheter has a significant risk of being misinterpreted [23]. The high learning curves involved with endovascular catheterization are another risk. Synthetic models, animals, cadavers, and virtual reality (VR) simulators are some of the teaching approaches used in this field [24, 25, 26].

1.1.4 Clinical Need for Force Feedback

Guidewire oversteering and rupture in the arteries or heart chamber can occur if the surgeon does not have a good sense of touch [27]. Other studies described the robotic intervention as a costly procedure that most persons with cardiac problems cannot afford [28]. It is

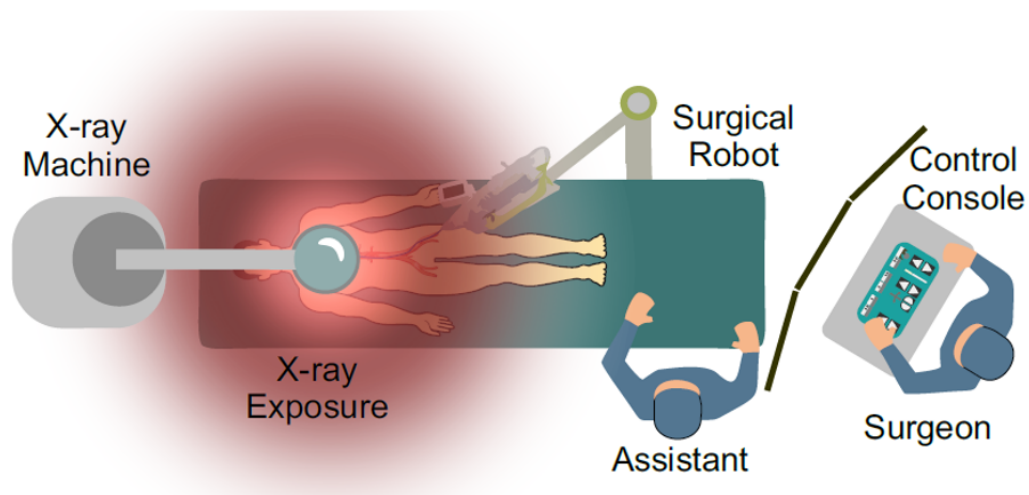


Figure 3: robot-assisted cardiovascular intervention [22]

worth noting that, despite the opposing viewpoints in robotic-assisted novel approaches, the quantity and diversity of treatments are growing [29]. When it comes to the relevance of force feedback, a study has shown that keeping the contact force between the ranges of 20 ± 10 grf is critical for the success of robotic operations [30]. Two significant ways for providing haptic feedback in teleoperations have been developed: sensor-based and model-based, or in other words, direct and sensorless techniques. The first option is to place a sensor at the contact site and detect the forces and torques [31], which could then be reproduced in a separate module distant from the patient to provide feedback to the surgeon. When constructing force sensors for sensing contact force, thickness, flexibility, sensitivity, and mass-fabrication capabilities are essential considerations. Normal and tangential forces should be detected by force sensors used in RF ablation catheters, and only a few research have been conducted to create such force sensors [32]. Valdastrì et al. developed a cutting tool incorporating triaxial force-sensing for minimally invasive procedures in 2007 [33]. The sensor's outside diameter was less than 3 mm, allowing it to be put through a 9 French catheter guide. Ex-vivo muscle tissue cutting studies were used to assess the sensor's performance. The third option is to calculate the force and estimate it using a computer model

[34]. Regarding RFA limitations, it is worth noting that longer procedure times are linked to consequences such as asymptomatic cerebral lesions (ACL) and perforation, and it was observed to occur in roughly 41% of individuals after RF ablation [35].

1.2 Literature Review

1.2.1 Modeling a catheter as a soft robot

Three broad groupings of probable design techniques for robots have been presented based on the comprehensive design options [36]. The first set of robots classified as conventional manipulators are discrete robots. The number of separate joints enhances the manipulator's DOF and mobility, resulting in the second category of robots, known as serpentine robots. Hyper-redundant manipulators fall under this group. The third type of robot is a continuum robot because it lacks distinct joints and stiff linkages. The manipulator, like biological trunks and tentacles, constantly bends along its length. Unlike traditional robots, which create motion at discrete joints, the motion of the final group is achieved by bending the robot across a specific segment. Model-based haptic feedback [22] is a type of continuum model in which the force is approximated using computing, live imaging, sensor boundary conditions, and a mechanical model of the catheter. Nakamura et al. [37] were the first to introduce a system that used high-speed cameras and tracking markers mounted on the heart surface to assess heart motion using a vision sensor. Because the output and findings are directly tied to the treatment and life of the patient, a real-time and precise solution is required to avoid any potential patient harm [38]. Different continuum models for continuum robots were introduced, for example, in 2003, a continuum backbone section enduring a considerable deflection was studied based on the dynamics of a planar, and a vibration-damping setpoint controller was established on this very dynamic analysis [39]. Bryan. A. et al. published a new approach for kinematic analysis of Multisection

Continuum Robots in 2006 [40]. By mapping inputs like tendon lengths or pneumatic pressures to robot shape, kinematics allows real-time shape control. In the final results, the new technique took into account bending and varied orientations. By ignoring shear effects and out-of-plane warping of the cross-section due to the catheters' great slenderness, Bernoulli-Euler beam theory was employed to analyze the large deflection of a steerable catheter. This approach was proved to be capable of successfully predicting the contact force at the tip of the catheter in a steady-state situation, with an error claimed to be less than 5% [41]. Although the findings were promising, their model did not adapt to numerous point loads or wall contact circumstances during a robotic PCI. Gao et al. [26] suggested a linear finite element model using Bernoulli-Euler elements to predict the contact force in their virtual reality-based Robotic Catheter System for training purposes.

The second group is Multi-body dynamics models, which are effective because of their simplicity and computational efficiency [22]. Different groups have proposed a semi-analytical methodology to simulate guidewire motion in the vasculature with two key components, such as the finite element method (FEM), mass-spring modeling approach, and multi-body dynamics [42]. A new method for describing guide wire forms, as well as a two-dimensional parameterization of the guidewire. The final findings were said to be in good accord with the experimental findings. In 2009, Ganji et al.[17] suggested a Multi-body dynamics model with stiff linkages and joints to forecast catheter tip location under the assumption of continuous catheter curvature. The FEM computing procedure is often time-consuming, but it is also realistic [43]. Tissue modeling has been shown to benefit from mass-spring models. The majority of existing research in this area is based on root mean squared error (RMSE), but only a few have looked at dice similarity coefficient [44]. They also proposed a hybrid mass-spring model with mass particles connected by non-bendable springs, as well as a multi-body system made up of rigid bodies and joints. Because a robot comprises numerous elements connected by joints, multibody dynamics

is a good fit for controlling it [45, 46]. A. Shabana published a comprehensive study of flexible multibody dynamics in 1997 [47]. It is shown that multibody dynamics is an interdisciplinary field encompassing rigid body dynamics, continuum mechanics, finite element technique, and numerical, matrix, and computer approaches. The three primary techniques utilized in flexible multi-body dynamics are the floating frame of reference formulation, the incremental finite element formulation, and the large rotation vector formulation.

The third group is particle-based dynamic models, which are mostly used to mimic the deformation of vascular tissue, as well as catheters and surgical instruments [48]. It is a macroscopic approximation of a continuous, in a sense. To properly approximate a catheter, angular springs were put in between consecutive stiff linkages. Haptic feedback and accurate force feedback control are two important variables in recreating the behavior of tissue in contact with the catheter in a robotic surgical interventional procedure [49]. Model-free and model-based approaches are the two primary types of vessel segmentation techniques [50]. For example, C. Florin used a particle-based technique to describe the full segmentation of the coronaries [5]. On the other hand, S. Cotin developed a physics-based model consisting of a collection of linked beam components, a particle-based technique to model and analyze the catheter, capable of simulating bending, twisting, and other deformations in real-time [50].

1.2.2 Geometric models

A deformable structure's dynamic equations, whether in large or small deformation, are extremely nonlinear. Modern digital computers play a significant role in studying flexible body structures because of their nonlinearity and huge dimensionality [47]. The essential premise in geometric modeling is that the entire structure and shape rely on the location of some specified points on the structure, known as critical points. However, the key points

are not totally located on the structure and might be anywhere in space. Piecewise differentiable continuous curves exemplify this approach for analyzing the structure of steerable catheters. Motion equations might be derived using the Lagrangian equation of motion based on kinetic, potential, and friction or viscoelastic energies depending on the stated critical points [22]. In terms of dynamic analysis, a flexible beam, such as a soft robotic arm or a steerable catheter (which is considered a beam), has an unlimited number of degrees of freedom. Therefore, it is attempted to minimize the number of degrees of freedom (DOF) needed to represent displacements and deformations by modeling [51, 52]. The guidewire was simulated, and the ultimate location of the guidewire was estimated using a series of linked vertices [53], which depended on fundamental physics. By applying the identical forces to the vertices, the sets of vertices replicate the guidewire. After a few rounds, the forces are in equilibrium, and the least energy position is obtained. Wen. T. et al. used the nonlinear elasticity of the Cosserat rod in 2012 [54]. The Cosserat centerline curve was utilized to simulate the instrument's bending and twisting. The instrument's distal tip is shorter and more flexible (3 cm), and it is modeled using a more computationally efficient generalized bending model.

1.2.3 Force Feedback Rendering for RCI

As mentioned before, Cardiac Arrhythmia has been one of the most causes of hospitalization in terms of cardiac-related disease. The catheter ablation procedure, which has been widely adopted as an effective interventional treatment for atrial fibrillation (AF) and has expanded widely from the initial stages of investigation to a commonly performed ablation procedure in many health centers throughout the world [55],[56]. During the ablation, arrhythmic cardiac cells are inactivated by either freezing (cryo-ablation) or burning (radio-frequency ablation). Robotic catheter intervention (RCI) systems have been widely designed and introduced [57], where the surgeons lose the direct touch on the catheter and

the contact, the force needs to be estimated for the sake of effective treatment [58]. Minimally invasive surgery (MIS) has revolutionized in treatment of atrial fibrillation (AF) that researches across the world carried out researchers to increase the dexterity in MIS procedures and priority is given to MIS over conventional surgeries because of less discharging time of the patients and minimal lesion, minimizing trauma specifically for those suffering from anemia. Lack of haptic (force and tactile) feedback provided to the surgeons is considered as a major limiting factor in MIS. While catheterization, the excessive force could hurt the damaged tissue, and insufficient force may result in a half-baked treatment[59][60]. Studies have shown that to have by monitoring the changes in the shape of the deflectable distal shaft of the catheter effective treatment and to avoid tissue perforation maintaining a stable constant force at the range of 0.1–0.3 N, is necessary [22].

Despite all the benefits offered by MIS, this procedure suffers from one significant restriction: the shortage of the force control. Force control falls into force measurement and force estimation. piezo-resistive [61, 62], Optical[63, 64], piezo-electric[65, 66], and capacitive[67, 68] materials could provide accurate force feedback in catheterization procedures. To measure the force at the point of contact between the cardiac tissue and surgical device, a force sensor could be deployed [69], where a miniaturized Piezo Force Sensor was used to measure the force. Some sensor-less force estimation methods were deployed [70], where the feasibility of the force estimation was investigated using investigates the feasibility of estimating the force that the catheter tip in touch with the heart tissue. To forecast the force at the contact point various methods were deployed such as heuristic methods [45], where a displacement-based viscoelastic model was introduced. Other researchers proposed that the data on the contact-tissue force can be accumulated from the variations in the catheter's position/shape and orientation of the distal, where the contact-tissue force can be controlled by altering the flexion of the distal shaft [70, 41, 71].

In comparison, sensor-based techniques provide high accuracy, refresh rate, and response time to the surgeons. While model-based approaches are less complicated, more adaptable, and significantly cheaper, and mainly supply more information about the state of distributed force and deformation throughout the catheters. Sensor-less methods are mathematically complicated in simulating the catheters and guide-wires and requiring the extraction of catheters' mechanical properties, vessels, and motion of the vasculature discretization length [22]. The implementation of sensors to obtain the force feedback at the catheter tip requires miniaturizing the sensor over the cardiovascular catheter. This may carry barriers to manufacturing the sensors in terms of sizing, MRI compatibility, and the catheter's structural flexibility. In contrast with model-based approaches, sensor-based methods are less dependent on unknown mechanical characteristics such as the catheter's stiffness or structure. They can provide fast feedback to the surgeons[72]. It is worth noting that sensor-embedded catheters' availability, high cost, and sterilizability are considered the premiere limitations of sensor-based techniques[73].

1.2.4 Force Estimation: Haptic Cue

Computer-controlled systems that mix discrete and continuous phenomena are known as haptic interfaces. The force feedback occurs in a distinct virtual area, but the human-device contact occurs continually. Real or virtual interaction can generate rendered forces (as in virtual reality simulation). The control and stability difficulties in force feedback are always the same, regardless of the type of the initially displayed interaction [74]. The motor driving current is proportional to the force feedback for the most known devices that adopt impedance like physical systems [75]. It is usually sufficient to utilize open-loop force control to feedback the force [76]. However, because the rendered forces quality is strongly impacted by these concerns, actuation and transmission system selection should

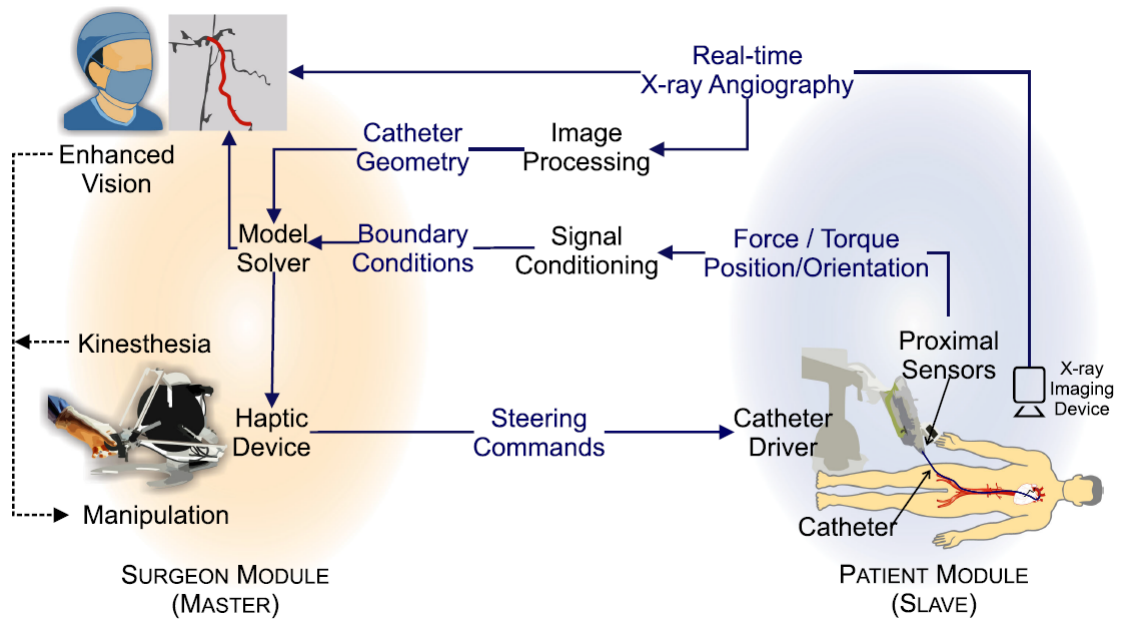


Figure 4: model-based haptic feedback approaches [77]

be carefully considered in the design process to offer low friction, backlash-free, well-compensated gravity effect master console. Clinical trials have raised serious concerns regarding the lack of haptic input during robotic operations [78, 79]. For example, Seto et al. [80] and Smilowitz et al. [21] compared the haptic feedback-free robotic intervention to blind catheter and guidewire control. Furthermore, the lack of haptic input in robotic intervention is associated with poor hand-eye coordination [81]. As a result, a surgeon's geometric vision of the catheter and vessels is hampered and the excessive contact force between the catheter and the vascular wall has been linked to a significant risk of embolization, perforation, thrombosis, and dissection in studies [49, 82, 23]. Uncertainty concerning the catheter insertion force and depth has been cited as a reason for robotic treatments being halted. For example, Rafii-Tari et al. [23] recently discovered that beginner and experienced interventionists in five frequent robotic interventional procedures had considerably distinct force-time signatures. They also discovered that the pulling force for beginners was up to six times greater than for professionals. On the other hand, other studies have

found that delivering force feedback to a surgeon during simulated aortic cannulation can reduce the contact force between the catheter and the aorta by up to 76 percent [83].

Sensor-based and model-based also known as direct and sensorless, haptic teleoperation for robotic interventions have been implemented utilizing two unique methodologies. The haptic forces and torques, also known as haptic feedback, are used in the sensor-based method. Sensors in the patient module (slave) measure haptic cues, which are then duplicated (rendered) by a haptic device in the surgeon module (master). The haptic stimulation is calculated using a computer model in the model-based method [34]. (see Fig. 4). In addition, a mechanical model of the catheter (and guidewire) is frequently included and an image processing engine for shape sensing and a force/torque estimate module. However, proximal force/torque and position/orientation inputs are required in the model-based method to limit the model with correct boundary conditions. Force/torque sensors and position/orientation encoders are used to receive such feedback. The model formulation and solution schema dictate which boundary condition is used [49]. Fig. 4 depicts the system architecture for model-based haptic telerobotic cardiovascular intervention.

The method of reproducing estimated or measured forces for a computer user to experience the true feeling of an item is known as haptic rendering [34]. The haptic device is the device with which the user interacts and which forces are created and conveyed to the user's hand. As seen in Fig. 4, haptic rendering is achieved using a closed-loop force control system. Many haptic devices have been proposed for robotic intervention, such as general-purpose multiple-DOF devices and custom-designed devices.

Six-DOF Phantom devices (3DSystems Inc., SC, US) were among the first systems to be employed as control and haptic interface for active catheter insertion [84]. Similarly, catheter insertion forces have been relayed to the surgeon's hand using Omega haptic devices (Force Dimension, Nyon, Switzerland) [85]. Phantom devices are built as serial

robotic mechanisms that create torque and force feedbacks using numerous capstan mechanisms and separate DC motor current management (one motor per DOF). This architecture enables this device family to offer a broad kinematic range in working space. However, the total system rigidity, has been weakened by the serial architecture.

On the other hand, the Omega device is built on a delta-based parallel mechanism that regulates forces and torques by controlling current on several motors at the same time. The device's stiffness has been enhanced, and it has become fundamentally symmetric along the X, Y, and Z axes. On the other hand, Omega devices have a smaller workspace. Nonetheless, within the catheter insertion force range (0-2N), and spatial resolution (0.1 mm) [23], both devices provide dependable industry-standard solutions for haptic feedback. Both systems are very well-maintained, and manufacturers provide extensive software development kits (SDK). The SDKs allow a designer to operate the device at both high-level (requiring the least programming abilities) and low-level (requiring greater programming abilities). Clinicians think that using a pen-like (stylus) interface for robotic intervention, as employed in the Phantom and Omega systems, is counter-intuitive for surgeons and will result in lengthier learning curves [58, 80]. As a result, researchers have created intuitive haptic interfaces to satisfy better clinical needs [86].

For force control and haptic rendering, studies have looked at active, semi-active, and passive actuation [86]. The type of actuation to use is significantly dependent on the application and the required force range. For example, the haptic device can comply freely with the user (at zero current) or aggressively resist the user's movements using active actuation, such as DC motors (at the maximum current). Active actuation, on the other hand, is susceptible to instability, backlash, force inadequacy, and jitter, as well as energy loss [87]. Therefore, the use of semi-active actuation to improve the stability of motor-driven devices has been proposed. It is accomplished by using a DC motor and a mechanical brake at the same time. The integrated brake dampens the system's vibrations and improves stability

[88]. However, it comes at the cost of a reduced peak force and decreased agility [87, 88]. Haptic rendering is achieved in passive actuation by modulating the resistance to motion, such as viscous friction on the catheter. Yin et al. [87, 89] used a medium filled with a magneto-rheologic-fluid (MRF) as the haptic interface. A catheter was inserted into the medium, and the current in a coil encircling the medium was used to alter the viscosity of the MRF. As a result, viscous friction on the catheter (resistance to motion) was adjusted so that the user's total insertion force equals that measured on the slave side [89]. Nevertheless, the development of haptic interfaces is still in its infancy, and it is expected that the introduction of wearable haptic solutions will open a new front for a more intuitive haptic supply for cardiovascular intervention.

1.3 Problem Definition

As mentioned before, during the last five years, robot-assisted cardiovascular intervention (RCI) systems have been introduced to reduce the health risks for patients and surgeons. RCI systems typically are teleoperated system with leader-follower system architecture that have moved the surgeon to a few meters away from the X-ray source. RCI has significantly reduced the risk factors for surgeons. However, clinicians have identified the lack of force feedback as its main technological limitation. The objective of this thesis was to develop, verify, and validate mechatronics technology for real-time accurate and robust haptic feedback rendering for RCI systems. The focus of the studies in this thesis was on robot-assisted catheter ablation procedure which is amongst the most recently adopted RCI procedures.

1.4 Research Objectives

Since the original motivation of this work was to develop, verify, and validate mechatronics technology for real-time accurate and robust haptic feedback rendering for RCI systems, the objectives of this research were categorized into three main groups.

- (1) To develop, implement, and validate the force estimation method to estimate contact force along with the endovascular devices that is accurate with less than 10% full-scale error within the operational range of contact forces, i.e., 0–0.2 N..
- (2) To develop a mechanistic model for tendon-driven ablation catheters to simulate the deformation of the ablation catheter in contact with atrial tissue that can be solved fast to perform in real-time, i.e., the minimum refresh rate of 25 Hz.
- (3) To develop, implement, and validate an intuitive haptic enabled surgeon module that shows enhanced stability, robustness, and accuracy in the presence of communication disruption. It should exhibit a haptic rendering refresh rate of at least 25 Hz and be accurate with less than 10% error of the desired force.

1.5 Research Scope

- (1) Developing a force estimation method for endovascular devices based on training multiple learning-based models in a learn-from-simulation framework by simulation dataset of the deformation of the ablation catheter in contact with atrial tissue.
- (2) Developing a new mechanistic model i.e., finite arc method (FAM) for tendon-driven ablation catheters based on mechanics of soft robots.
- (3) Developing a novel impedance-based force feedback rendering modality to represent teleoperated RCI system for experimental validation that can enhance stability,

robustness, and accuracy in the presence of communication disruption.

1.6 Contributions

The following list summarizes the author's contributions during this master research:

- (1) Amir Sayadi, Hamidreza Nourani, Mohammad Jolaei, Javad Dargahi, and Amir Hooshidar. Force Estimation on Steerable Catheters through Learning-from-Simulation with ex-vivo Validation. *In the 2021 International Symposium on Medical Robotics (ISMR) hosted on the campus of Georgia Tech from 17-19 November, Atlanta, USA, In-press, 2021,*
- (2) Amir Sayadi, Javad Dargahi, Renzo Cecere, and Amir Hooshidar. Mechanical Modeling and Analytical Solution of Soft Tendon-Driven Robots with Large Deformation: Finite Arc Method (FAM). *In the IEEE International Conference on Robotics and Automation (ICRA) from 23-27 May, Philadelphia (PA), USA, under review, 2022.*
- (3) Amir Sayadi, Amir Hooshidar, Javad Dargahi. Impedance Matching Approach for Robust Force Feedback Rendering with Application in Robot-assisted Interventions. *In the 8th International Conference on Control, Mechatronics and Automation (IC-CMA), Moscow, Russia, pages 18-22, IEEE, 2020 [90],*
- (4) Amir Hooshidar, Amir Sayadi, Javad Dargahi, and Siamak Najarian. An integral-free rotation measurement method via stereo-accelerometry with application in robot-assisted catheter intervention. *IEEE/ASME Transactions on Mechatronics, 2021 [91],*
- (5) Amir Hooshidar, Amir Sayadi, Javad Dargahi, and Siamak Najarian. Analytical tip force estimation on tendon-driven catheters through inverse solution of cosserat rod

model. *In International Conference on Intelligent Robots and Systems (IROS), 2021*, IEEE, In-press, 2021 [92],

- (6) Amir Hooshier, Amir Sayadi, Mohammad Jolaei, and Javad Dargahi. Accurate estimation of tip force on tendon-driven catheters using inverse cosserat rod model. *In 2020 International Conference on Biomedical Innovations and Applications (BIA)*, pages 37–40. IEEE, 2020 [93],
- (7) Mohammad Jolaei, Amir Hooshier, Amir Sayadi, Javad Dargahi, and Muthukumaran Packirisamy. Sensor-free force control of tendon-driven ablation catheters through position control and contact modeling. *In 2020 42nd Annual International Conference of the IEEE Engineering in Medicine & Biology Society (EMBC)*, pages 5248–5251. IEEE, 2020 [56],
- (8) Majid Roshanfar, Amir Sayadi, Javad Dargahi, and Amir Hooshier. Stiffness adaptation of hybrid soft surgical robot for improved safety in interventional surgery *In the 2022 ACM/IEEE International Conference on Human-Robot Interaction from 7-10 March, Sapporo, Hokkaido, Japan*, under review, 2022.

1.7 Thesis Layout

This thesis is prepared in manuscript-based style according to the "*Thesis Preparation and Thesis Examination Regulations for Manuscript-based Thesis*" of the School of Graduate Studies of Concordia University, and consists of the following chapters:

Chapter 2: presents a real-time tip force estimation method based on image-based shape-sensing and learning-from-simulation is provided. To this end, a generalized image-based shape-sensing technique for flexural robots was developed using the Bezier spline interpolation method. Afterward, the deflection of a commercial catheter subjected to a series

of tip forces was simulated using nonlinear finite element modeling. Next, two independent data-driven models, i.e., artificial neural network (ANN) and support vector regression (SVR), were trained with a dataset with the Bezier spline control points as the inputs and tip forces as the output. For validation, the trained models were used for real-time tip force estimation while the catheter was pressed against porcine atrial tissue. The test was performed using a universal testing machine that recorded the groundtruth contact force. This chapter is based on a manuscript accepted in the *2021 IEEE International Symposium on Medical Robotics (ISMR) hosted on the campus of Georgia Tech*:

- Amir Sayadi, Hamidreza Nourani, Mohammad Jolaei, Javad Dargahi, and Amir Hooshidar. Force Estimation on Steerable Catheters through Learning-from-Simulation with ex-vivo Validation", in The 2021 International Symposium on Medical Robotics (ISMR) hosted on the campus of Georgia Tech from 17-19 November, Atlanta, USA, In-press, 2021.

The second and third author of this manuscript assisted in the preparation of the experimental setup and the fifth author was an academic advisor. The contents of this manuscript were not used by any of the co-authors in their graduate theses.

Chapter 3: presents a new mechanistic model, i.e., finite arc method, for planar soft flexural robots with external driving, e.g., tendon-drive, was proposed and validated. To this end, first the robot was modeled as a finite number of arcs, each with a constant bending curvature, hence the name finite arc methods (FAM). Afterwards, using Bezier shape approximation method, the deformation was parameterized and the kinematics and balance equations of the robot were derived. To find the deformation of the robot, a sequential algorithm was proposed. The deformed shape of the catheter was then reconstructed by serially constructing the arcs from the base toward the tip of the flexural robot. This chapter is based on a manuscript under review in *IEEE International Conference on Robotics and Automation (ICRA)*, Philadelphia (PA), USA:

- Amir Sayadi, Javad Dargahi, Renzo Cecere, and Amir Hooshier. Mechanical Modeling and Analytical Solution of Soft Tendon-Driven Robots with Large Deformation: Finite Arc Method (FAM). *In the IEEE International Conference on Robotics and Automation (ICRA) from 23-27 May, Philadelphia (PA), USA*, under review, 2022.

The third and fourth authors of this manuscript contributed as scientific advisors.

Chapter 4: presents an impedance-based force feedback approach was proposed and validated. Initially a fast impedance identification method for estimating the impedance of cathetervasculature interaction at the slave module of such systems was obtained. Afterward, a force feedback approach based on matching the mechanical impedance of the master module with the identified impedance was implemented. The proposed force control method was experimentally studied for a robotassisted remote catheter insertion task. Also, the performance of the proposed method was experimentally compared to the conventional direct force reflection approach. This chapter is based on a manuscript presented during *the 8th International Conference on Control, Mechatronics and Automation (IC-CMA), Moscow, Russia, IEEE, 2020*:

- Amir Sayadi, Amir Hooshier, Javad Dargahi. Impedance Matching Approach for Robust Force Feedback Rendering with Application in Robot-assisted Interventions. *In the 8th International Conference on Control, Mechatronics and Automation (IC-CMA), Moscow, Russia,, pages 18-22, IEEE, 2020 [90]*.

The second author of this manuscript contributed as an academic advisor.

Chapter 5: This chapter demonstrates the conclusions and proposed extensions for the future works, which can be carried by referring to the current study.

Chapter 2

Tip Force Estimation on Soft Flexural Robots through Shape-sensing and Simulation-based Training with *ex-vivo* Validation

Monitoring and control of the contact force at the tip of soft flexural robots is of high application need, e.g., the tip force on radiofrequency ablation (RFA) catheters. In this study, a real-time tip force estimation method based on image-based shape-sensing and learning-from-simulation is provided. To this end, a generalized image-based shape-sensing technique for flexural robots was developed using the Bezier spline interpolation method. Afterward, the deflection of a commercial catheter subjected to a series of tip forces was simulated using nonlinear finite element modeling. Next, two independent data-driven models, i.e., artificial neural network (ANN) and support vector regression (SVR), were trained with a dataset with the Bezier spline control points as the inputs and tip forces as the output. For validation, the trained models were used for real-time tip force estimation while the catheter was pressed against porcine atrial tissue. The test was performed using a universal testing machine that recorded the groundtruth contact force. The comparison showed that the ANN model had a mean-absolute-error of 0.0217 ± 0.0191 N, while the SVR model exhibited a mean absolute error of 0.0178 ± 0.0121 N and a correlation coefficient of 0.991. Moreover, the proposed method showed a minimum computational refresh

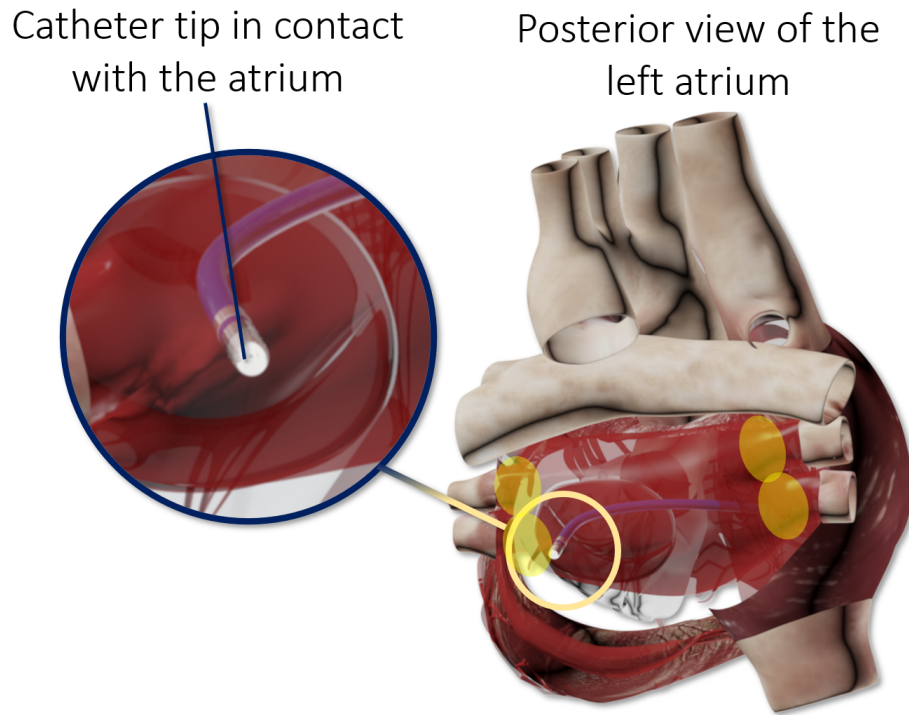


Figure 5: Catheter ablation for atrial fibrillation

rate of 646 Hz (ANN) and 917 Hz (SVR) during the validation experiment. The performance of the proposed method was in compliance with the clinical requirements of RFA therapy.

2.1 Introduction

2.1.1 Background

Cardiac arrhythmia caused by atrial fibrillation (AFib) is one of the most prevalent cardiac diseases and can result in embolism, myocardial infarction, and death. The catheter ablation approach, e.g., radiofrequency ablation (RFA), cryoablation (CRA), and pulsed-field ablation (PFA), has become the gold-standard treatment for AFib worldwide [22]. During the ablation, undesired electrical pulsations within the atrium and around the pulmonary vein entrance to the atrium are suppressed through atrial ablation. Atrial ablation involves

degeneration of the atrial tissue through cold or hot burning or through electroporation phenomena. Secondary to ablation, the atrial tissue becomes electrically inert and blocks the propagation of undesired electrical pulses from pulmonary veins into the atrium.

Atrial ablation is typically performed using manual catheters, however, robotic catheter intervention (RCI) systems have been introduced in the last decade for more precise mapping and ablation tasks [57, 22]. One of the technical challenges of ablation therapy has been the inability to precisely control the contact force between the catheter tip and atrial tissue [58, 22]. To alleviate this limitation, studies have proposed using sensor-equipped catheters using piezoresistive [69, 94, 46], piezoelectric [65], capacitive [68] and optical-based sensors [64, 95]. Nevertheless, the cost burden, manufacturability, and miniaturization have limited the adoption of sensor-equipped catheters by clinicians.

As an alternative, the sensor-free approach, especially image-based force estimation based on shape-sensing, has been proposed in the literature [77]. Such methods typically rely on a heuristic or mechanistic model of the catheter. The model is solved inversely to find the unknown tip contact forces using the real-time images of the deflected catheter. In a series of early studies, Khoshnam *et al.* [70, 71] showed the feasibility of image-based force estimation using a heuristic Gaussian mixture model. Their results however were not to the desired accuracy for clinical validation mainly due to the model insufficiency. In another study, Back *et al.* proposed a mechanistic inverse model of the RFA catheter and showed favorable accuracy in planar in-vitro tests. However, their method relied on tracking fiducial markers on the catheter that might not be possible with X-ray fluoroscopy images. In recent studies, Jolaei *et al.* [56, 45, 96] proposed a hybrid learning-mechanistic method for displacement-based control of contact force on RFA catheters. Their results showed force control with more than 85% accuracy and 90% repeatability. Nevertheless, the mechanistic part of their model relied on real-time characterization of atrial tissue that might be prone to practical difficulty and error. Recently, the author proposed a mechanistic model of the

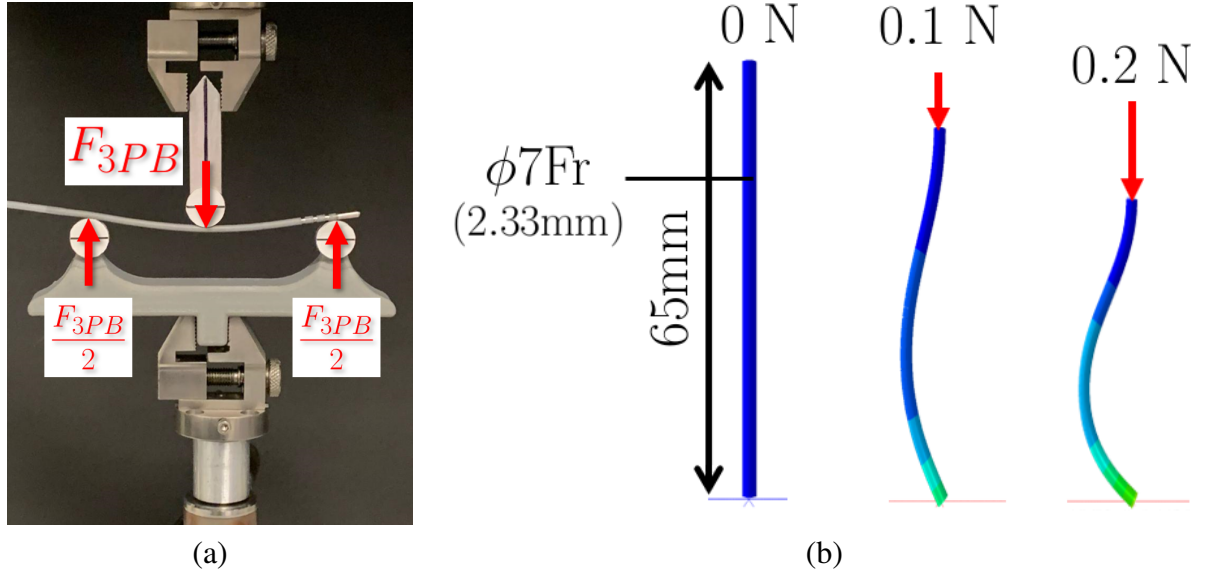


Figure 6: (a) Blazer II-XP under three-point-bending (3PB) test, (b) deformed shape of the catheter under axial loads.

catheter using Cosserat rod modeling and obtained a semi-analytical solution for it. Our results showed more than 90% accuracy in terms of force estimation. However, the developed Cosserat rod model was planar and relied on the single bending-radius assumption, thus, its real-world application may be limited.

2.1.2 Objective and Contributions

One of the remaining challenges, that have impeded the applicability of force estimation methods for practical use, is the complexity of mechanistic models and their susceptibility to parameter variation and inadequacy of learning-based models that require large training datasets. These factors have resulted in the complexity of integration of the models with existing catheterization systems, i.e., manual and robotic, and erroneous force estimation. To alleviate this problem, the objective of this study was to build upon the recently proposed learning-from-simulation approach to show the feasibility of generating accurate learning-based models trained by simulation data and assess its performance on real-world use-cases. The main contributions of this study are:

1. Building upon the accuracy of continuum mechanics-based deformation estimation of soft flexural robots and the speed of data-driven models for force estimation,
2. Providing a novel data-driven force estimation framework for tendon-driven soft robots based on simulation-based training,
3. proof-of-feasibility for the tip force control of tendon-driven flexural robots with the proposed force estimation method through *ex-vivo* validation.

2.2 Simulation and Shape Sensing

In this study, we initially developed and validated a finite element (FE) mechanistic model of a commercial RFA catheter and used it to generate a training dataset. Also, to encode the large deformations of the catheter (shape-sensing) a fast shape encoding method based on Bezier-spline interpolation was proposed. The proposed shape-sensing allowed for the reduction of input feature space (model-reduction) while encoded the deformation information efficiently. Afterward, two learning-based models, i.e., support vector regression (SVR) and feed-forward neural network (FFNN) were trained with the training dataset. Next, the trained models were tested for accuracy with a series of images taken from a commercial RFA catheter in contact with porcine cardiac tissue. In the following, the details of the performed study are provided.

2.2.1 Finite Element Simulation and Verification

To obtain the deformation of the RFA catheter in contact with atrial tissue, a planar FE model was developed and solved in Abaqus CAE, 2018 (ABAQUS inc, Dassault Systemes). The geometrical specifications of the catheter were obtained through direct measurements on a Blazer II-XP catheter (Boston Scientific, MA, USA). The model was 65

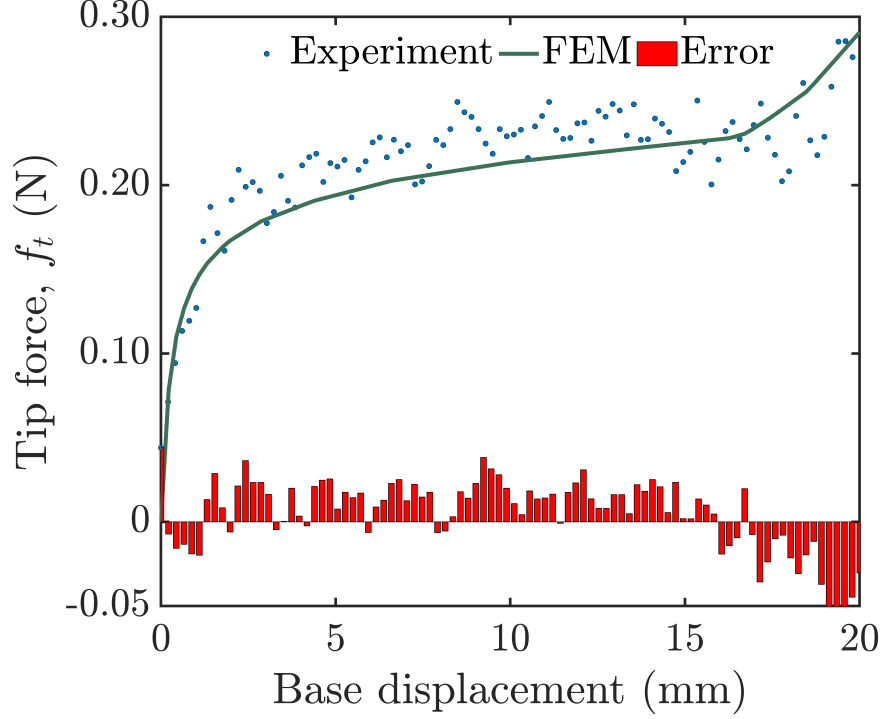


Figure 7: Comparison of force-displacement curve between the FE simulation and experiment.

mm long and with a hollow circular cross-section of 2.33mm (7Fr) outer and 1.75mm inner diameters. The flexural rigidity of the catheter, i.e., $EI = 60 \pm 11 \text{ Nmm}^2$ was measured through a three-point-bending (3PB) test per ISO 179:2019 standard (Fig. 6(a)). The model was meshed with 100 quadratic beam elements and was solved with a large deformation assumption. The tip of the catheter was in frictional contact with the ground. The coefficient of friction used in this simulation was 0.04 [97]. A base displacement of up to 20 mm was applied monotonically (ramp) to the base of the catheter. Fig. 6(b) depicts representative deformed shapes of the catheter under 0, 0.1, and 0.2 N axial loads. To validate the findings of the FE simulation, a similar test was performed on the catheter using a universal testing machine (ElectroForce 3200, TA Instruments, DA, USA). The displacement was applied with a rate of 1 mm/s. Fig. 7 compares the force-displacement curves obtained from the FE simulation and experiment. The comparison showed that the FE simulation

had an absolute error of 0.017 ± 0.011 N (5.6% of maximum force) in comparison with the experiment. Also, the force-displacement curves show the snap-through effect, identified by a rapid softening of the structure, at around the base displacement of 1.7 mm. The snap-through effect is an indicator of structural buckling under axial load on beams. In addition, the tip position did not move horizontally on the frictional ground surface that shows the sufficiency of the assumed friction coefficient. The similarity of the experimental result with the FE simulation verified the validity of the FE simulation, thus in continuation, the FE model was used to generate the training datasets for various axial forces.

2.2.2 Shape Sensing

From a physics point of view, beams can bend continuously along their centerline, thus have an infinite number of degrees of freedom (DoFs). As a shape sensing approach and to reduce the feature space for the learning-based models, a Bezier spline shape interpolation method was adopted from [98, 99]. The Bezier spline $\mathbf{c}(s)$ used in this study was of third-order and required determination of spatial coordinates of four control points, $\mathbf{p}_{0,1,2,3}$ in global coordination system. The author have previously derived the mathematical description of $\mathbf{p}_{0,1,2,3}$ to interpolate the shape of a segmented catheter as a circular arc in real-time images.

In this study, the shape of the catheter is not limited to be a circular arc and could deform arbitrarily. Thus, using the camera calibration matrix, obtained in Camera Calibration Toolbox of Matlab (R2020a, Mathworks, MA, USA), the spatial position of each segmented pixel in the image of the deformed catheter was obtained using:

$$\tilde{\mathbf{p}}_i = \begin{pmatrix} \tilde{x}_i & \tilde{y}_i & \tilde{z}_i \end{pmatrix}^T = \Psi_{3 \times 4} \begin{pmatrix} \tilde{u}_i & \tilde{v}_i & 0 & 1 \end{pmatrix}^T \quad i = 1 \cdots N, \quad (1)$$

where, N is the number of segmented pixels, $\Psi_{3 \times 4}$ is the camera calibration matrix. Also, there a unique normalized arc-length parameter s_i was defined for each pixel as:

$$\tilde{s}_i = \frac{\sum_{j=1}^{i-1} \sqrt{(\tilde{x}_{j+1} - \tilde{x}_j)^2 + (\tilde{y}_{j+1} - \tilde{y}_j)^2 + (\tilde{z}_{j+1} - \tilde{z}_j)^2}}{\sum_{j=1}^{N-1} \sqrt{(\tilde{x}_{j+1} - \tilde{x}_j)^2 + (\tilde{y}_{j+1} - \tilde{y}_j)^2 + (\tilde{z}_{j+1} - \tilde{z}_j)^2}}. \quad (2)$$

Prior to the arc-length calculation the segmented points were sorted using the Dijkstra algorithm [100]. According to [101, 98] the parametric discrete curve constituted by $\tilde{\mathbf{c}}(\tilde{s}) = \begin{pmatrix} \tilde{s}_i \\ \tilde{\mathbf{p}}_i \end{pmatrix}$ tuples can be uniquely fitted by a third-order continuous Bezier curve $\mathbf{c}(s)$:

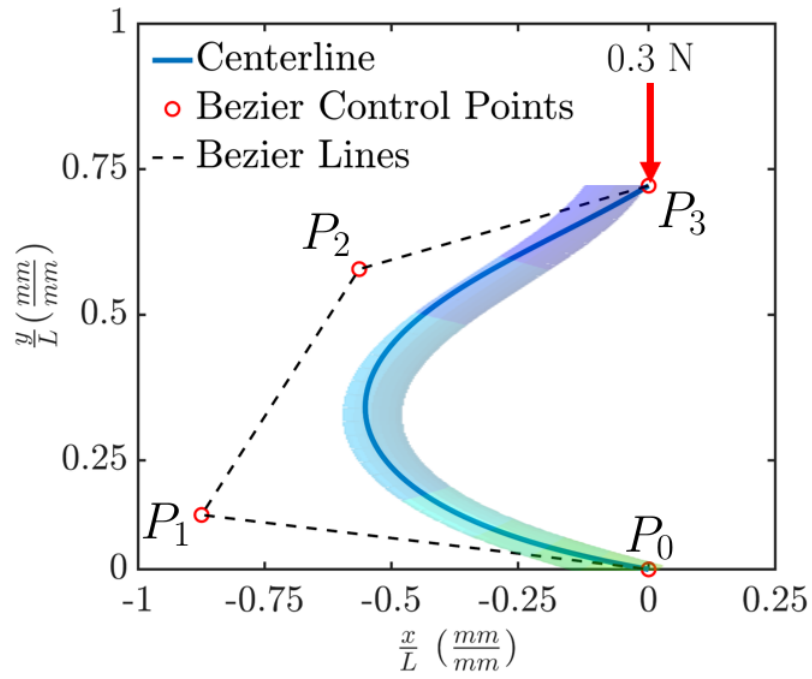
$$\mathbf{c}(s) = \begin{pmatrix} x(s) \\ y(s) \\ z(s) \end{pmatrix} = \begin{pmatrix} \mathbf{p}_0 & \mathbf{p}_1 & \mathbf{p}_2 & \mathbf{p}_3 \end{pmatrix} \begin{pmatrix} (1-s)^3 \\ 3s(1-s)^2 \\ 3s^2(1-s) \\ s^3 \end{pmatrix}, \quad (3)$$

with $s \in [0, 1]$. The author have shown in [98] that this shape fitting constitutes an over-determined least-square problem that has a unique Moore-Penrose non-trivial solution:

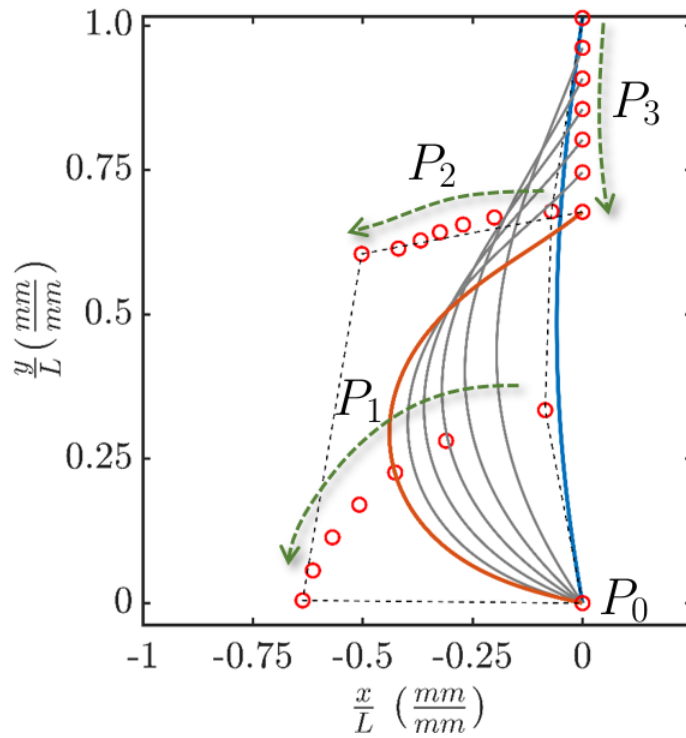
$$\begin{pmatrix} \mathbf{p}_0 & \mathbf{p}_1 & \mathbf{p}_2 & \mathbf{p}_3 \end{pmatrix} = \Gamma \Lambda^T (\Lambda \Lambda^T)^{-1}, \quad (4)$$

where,

$$\Gamma = \begin{pmatrix} \tilde{x}_1 & \cdots & \tilde{x}_N \\ \tilde{y}_1 & \cdots & \tilde{y}_N \\ \tilde{z}_1 & \cdots & \tilde{z}_N \end{pmatrix}_{3 \times N}, \quad \Lambda = \begin{pmatrix} (1 - \tilde{s}_1)^3 & \cdots & (1 - \tilde{s}_N)^3 \\ 3\tilde{s}_1(1 - \tilde{s}_1)^2 & \cdots & 3\tilde{s}_N(1 - \tilde{s}_N)^2 \\ 3\tilde{s}_1^2(1 - \tilde{s}_1) & \cdots & 3\tilde{s}_N^2(1 - \tilde{s}_N) \\ \tilde{s}_1^3 & \cdots & \tilde{s}_N^3 \end{pmatrix}_{4 \times N}. \quad (5)$$



(a)



(b)

Figure 8: (a) Representative shape of the deflected catheter and its corresponding Bezier curve, (b) Bezier shape fitting and Bezier control points for a representative set of catheter deformations.

To obtain the Bezier control points on simulated deformations from FE simulation, the deformed shapes of the catheter for force in the range of 0 to 0.3 N (force range of RFA ablation procedures [22]), were fitted using the proposed formulation. Fig. 8(a) depicts representative deformed shapes of the catheter from FE simulation with 0.3 N tip force and Fig. 8(b) shows a set of Bezier shape fittings on the simulated deformations for a monotonically increasing and vertical base force of 0 to 0.2 N. As indicated in Fig. 8(b) the Bezier control points spread wider as the catheter deflection increases. The post-processing showed that the shape fittings had a residual absolute error of 0.12 ± 0.05 mm between $\tilde{\mathbf{c}}(\tilde{s})$ and $\mathbf{c}(s)$. Thus, for each simulated load case, a unique set of $\mathbf{p}_{0,1,2,3}$ would describe the deformed shape of the catheter with acceptable accuracy.

2.3 Learning-based Force Estimation

2.3.1 Dataset

After validation of the developed FE simulation, a dataset was constructed with the position of Bezier control points p as inputs and the magnitude of the tip contact force f_t as the output. The input and output space were of the following form:

$$\text{input : } \mathbf{X} = \begin{pmatrix} \mathbf{p}_0 \\ \mathbf{p}_1 \\ \mathbf{p}_2 \\ \mathbf{p}_3 \end{pmatrix}_{12 \times 1} \quad \text{output : } y = f_t = \|\mathbf{f}_t\|, \quad (6)$$

where, \mathbf{X} , and y were the input and output vectors. To generate the dataset a total of 400 load cases corresponding to combinations of 16 base forces angles and 25 base force magnitudes were simulated. The base force angles were in the range of $[0, \pi]$ rad with an increment of $\frac{\pi}{16}$ rad and the force magnitudes were compressive in the range of $[0, 0.3]$ N

with an increment of 12 mN. For each load case, the Bezier control points were extracted using the method proposed in Sec.2.2.2. In the end, the dataset was compiled with the input and output vectors from 400 simulations and was randomly split with a 70:30 training-to-test ratio.

2.3.2 Model Selection and Training

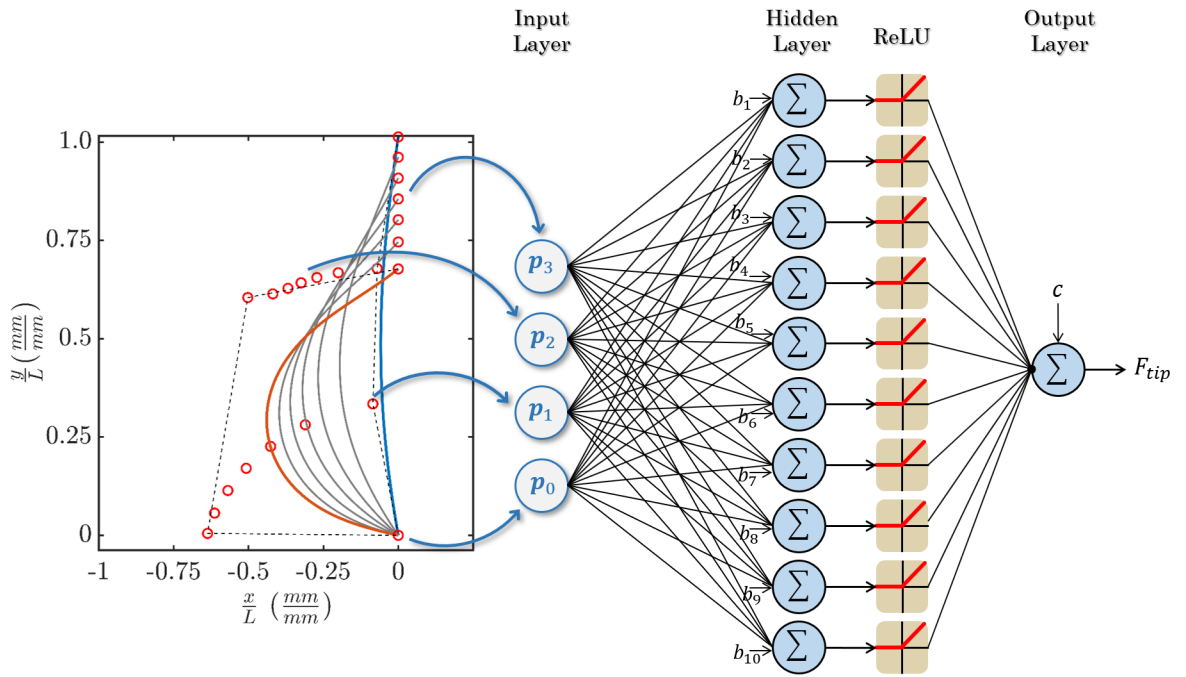
Mechanistic models have shown that the relationship between the forces on steerable catheters and their deformation is highly nonlinear, mainly due to nonlinear mechanical properties and large deformation [22]. Therefore, two well-established learning-based models were selected to test the hypothesis of this study. The selected models were support-vector-regression (SVR) and artificial (feed-forward) neural network (ANN).

2.3.2.1 ANN Model

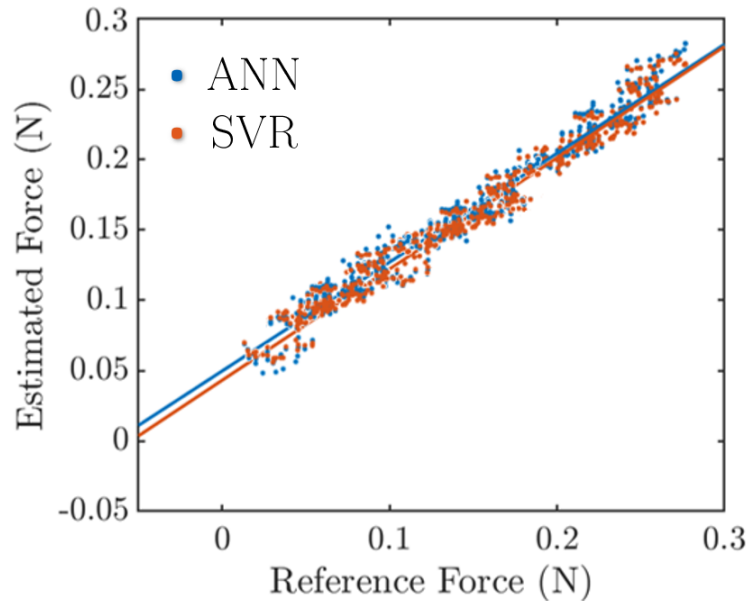
The utilized ANN model was of a single 12×1 input layer, a single hidden-layer, and a scalar output layer. The hidden layer had ten neurons each coupled to a rectified linear unit (ReLU) activation function. The number of hidden layers and neurons were selected manually and were the minimum that would result in a correlation coefficient of more than 0.995. Fig. 9(a) depicts the architecture of the ANN. The model was implemented in Python using the `sklearn` library and was trained with the training dataset ($n = 280$). After training the ANN model was tested for accuracy with the test dataset. The test statistics showed a mean absolute error of 0.0113 ± 0.0054 N and a correlation coefficient of 0.997 between the ANN prediction and training outputs (reference).

2.3.2.2 SVR Model

The utilized SVR model was nonlinear with a Gaussian kernel and a regularization parameter of $C = 100$. The regularization parameter was selected manually to enforce a



(a)



(b)

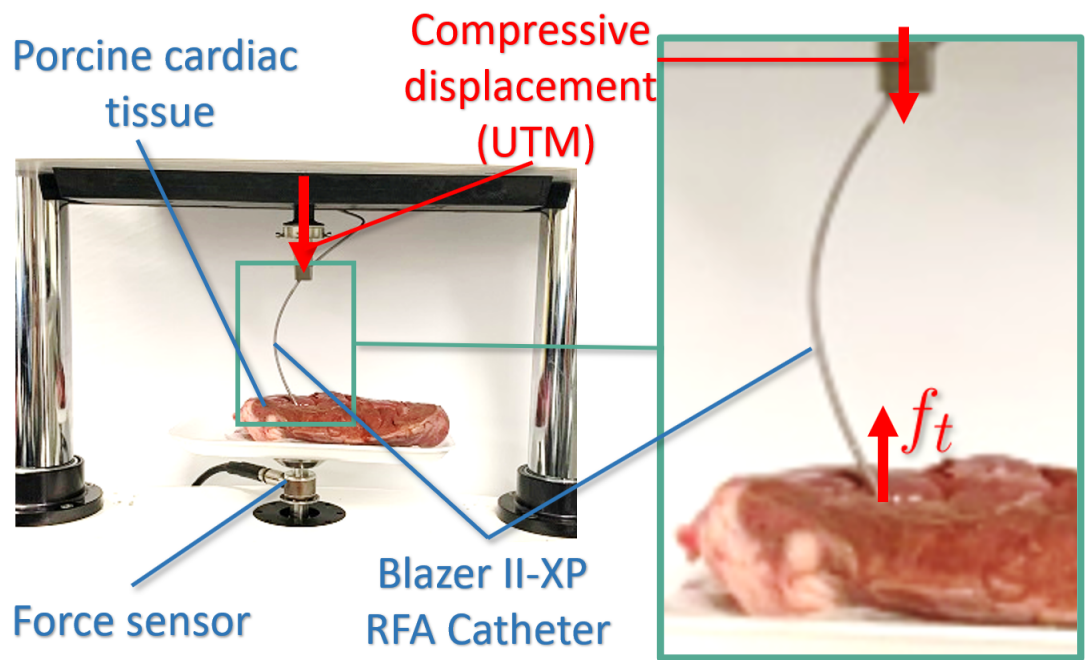
Figure 9: (a) Schematic architecture of ANN model for force estimation, (b) error of force estimation on test dataset for the trained ANN and SVR models.

minimum correlation coefficient of 0.995. The model was implemented in Python using the `sklearn` library. The model was trained with the training dataset ($n = 280$). After training the SVR model was tested for accuracy with the test dataset. The test statistics showed a mean absolute error of 0.010 ± 0.0161 N and a correlation coefficient of 0.995 between the SVR prediction and training outputs (reference). Fig. 9(b) shows the regression error for the ANN and SVR models.

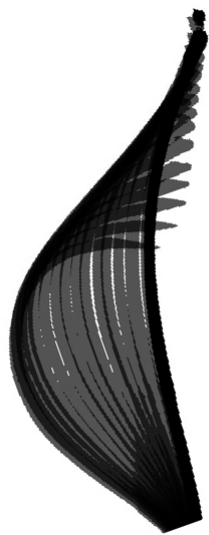
2.4 *ex-vivo* Validation Study

In order to investigate the feasibility of using the trained model for RFA ablation therapy, an *ex-vivo* test on a fresh porcine cardiac tissue was performed. Fig. 10(a) depicts the experimental setup used for *ex-vivo* validation. The catheter was fixed to the mobile (upper) jaw of the universal testing machine and was compressed on the tissue with a rate of 5 mm/s to reach a displacement of 20 mm. The catheter tip indentation on the tissue was approximately 6 mm (measured post-test). For each frame, the deflected shape of the catheter was obtained using the proposed method in Sec. 2.2.2. For each frame the catheter shape was extracted from binary segmented images (Fig. 10(b)) obtained through background removal and greyscale thresholding (threshold of 132 for 8-bit greyscale color-depth). Afterward, the Bezier control points were obtained, were used in ANN and SVR trained models for force estimation, and the model estimations were compared with the ground truth recorded by the universal testing machine. Fig. 10(c) shows the comparison of estimated force from ANN and SVR with the ground truth.

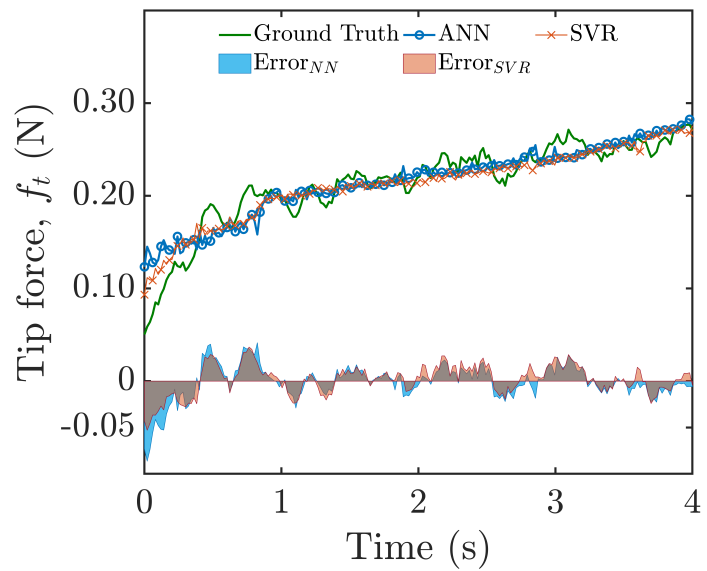
The mean absolute error (MAE) of the ANN model was 0.0217 ± 0.0191 N (7.2% of maximum force) with a root-mean-square error (RMSE) of 0.0191 N (6.4% of maximum force). For the SVR model, the MAE was 0.0178 ± 0.0121 N (5.9% of maximum force) with an RMSE of 0.0166 N (5.5% of maximum force). Also, the error distribution for both models was Gaussian (Fig. 11). The author deems the absence of multiple peaks and drastic



(a)



(b)



(c)

Figure 10: (a) *ex-vivo* validation test setup, (b) binary segmented shape of the catheter during *ex-vivo* test, and (c) comparison of the estimated force with ANN and SVR models with the ground truth recorded by the UTM.

skewness in the error distribution as an indicator confirming the adequacy of the models. It is noteworthy that since the catheter tip was indented into the tissue, the images could not fully capture the shape of the catheter near its contact with the tissue. This observation is evident in the binary images (Fig. 10(b)). Nevertheless, because of the choice of \mathbf{p}_0 at the tip of the catheter this phenomenon has not drastically affected the accuracy of force estimation. In clinical setups, the full shape of the catheter is visible in the X-ray images. Moreover, the minimum computational refresh rates of 646 Hz and 917 Hz were observed based on the computational time of the ANN and SVR models, respectively. Given that the frame rate of the fluoroscopy imaging devices is around 30Hz, the observed refresh rates were well beyond the requirement for real-time applications. The observed force estimation error was within the reported ranges of error in the literature, e.g. [71, 56] and was within the clinical requirement range, i.e., $< 10\%$.

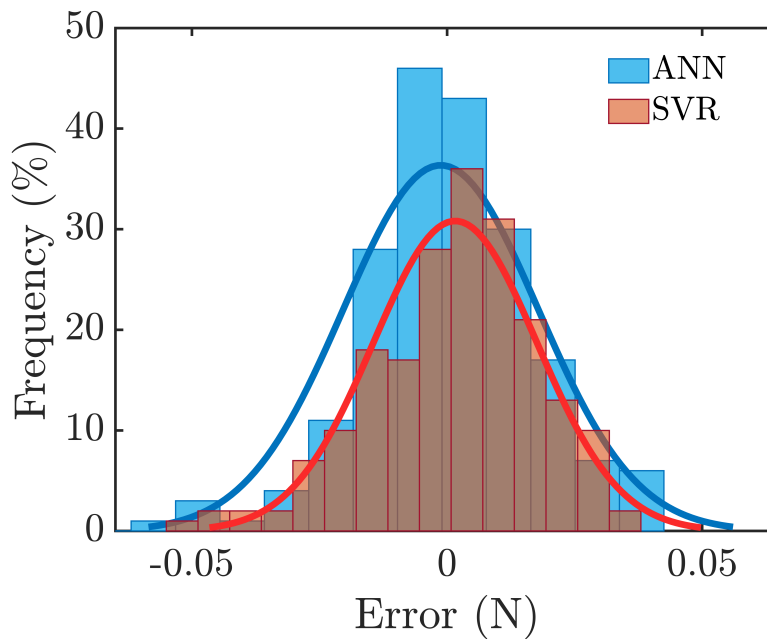


Figure 11: Distribution of force estimation error for ANN and SVR models in the *ex-vivo* test.

2.5 Summary

In this study, a new learning-based force estimation framework for steerable catheters based on the learning-from-simulation principle was proposed and validated. The utilization of a Bezier shape fitting method facilitated the reduction of input space dimensions for the models. The adopted nonlinear regression models, i.e., ANN and SVR were of acceptable accuracy within the clinical requirements range. One of the limitations of this study was the 2D deflection of the catheter that may not be valid in real surgical applications. However, the proposed shape interpolation method and the learning model architectures thereof allow for 3D shape interpolation and force estimation. In future studies, use of stereo-vision for 3D shape acquisition can contribute to the alleviation of this limitation. Another extension of this study would be to utilize the proposed method for haptic force rendering in combination with haptics-enabled remote intervention systems such as proposed in [90, 102, 91]. Also, replacement of the FE simulation with a less computationally costly method such as Cosserat rod modeling and direct incorporation of the Bezier shape interpolation with the model formulation, such as proposed in [98], may facilitate generation of larger training dataset for the inclusion of 3D load-cases.

Chapter 3

Mechanical Modeling of Soft Tendon-Driven Robots with Large Deformation: Finite Arc Method (FAM)

Accurate simulation of deformation of soft flexural robots, e.g., tendon-driven catheters, is of high clinical importance especially for the novel catheter-based interventions. In this study, a new mechanistic model, i.e., finite arc method (FAM), for planar soft catheters with external driving, e.g., tendon-drive, was proposed and validated. To this end, first the catheter was modeled as a finite number of arcs, each with a constant bending curvature, hence the name finite arc methods (FAM). Afterwards, using our recently validated Bezier shape approximation method, the deformation was parameterized and the kinematics and balance equations of the catheter were derived. To find the deformation of the catheter, a sequential algorithm was proposed. The deformed shape of the catheter was then reconstructed by serially constructing the arcs from the base toward the tip of the catheter. To validate the proposed method, two validation studies were performed. In Study I, the FAM's predicted deformations for eight load cases on a 40mm long flexure were compared with nonlinear finite element method (FEM). In Study II, a representative set of lateral forces on a cardiac catheter (obtained in our previous study) were used to find its FAM-based deformation and was compared with the experimental reference. The error between FAM and FEM deformations was $0.23 \pm 0.89\text{mm}$ with computation times of 3ms (FAM)

vs. 1244ms (FEM). Also, the error of FAM compared to ground-truth in Study II was 1.41 ± 1.47 mm with a computation time of 7ms. The proposed method showed acceptable performance for accurate prediction of highly complex large deformations in real-time.

3.1 Introduction

3.1.1 Background

Flexural robots are a class of soft robots that have been used in interventional robotics frequently. For example, flexural robots have been used in catheter ablation therapy in the left atrium [103]. This treatment has become the gold standard for the treatment of cardiac atrial fibrillation (AFib), the most prevalent cause of cardiac arrhythmia and the leading cause of hospitalization in cardiac electro-physiology [104]. Fig. 12 depicts a schematic view of the RFA catheter inside the atrium during ablation procedure. This procedure is minimally invasive thus the surgeon does not have direct vision on the trajectory of the shape of the catheter. Instead, they obtain such information through real-time x-ray imaging, i.e., fluoroscopy. To avoid the health risks associated with the x-ray exposure, remote leader–follower robotic platforms with tendon-driven catheters have been proposed recently [56]. Such systems have enabled surgeons to not only move away from the x-ray exposure risk zone but also do intervention from miles away [105, 106].

Similar to other novel medical technologies, simulation-based training is a clinical need for shortening surgeons' learning curve and increasing the adoption rate of flexural medical robots. To this end, having a fast and accurate computational model that can reliably predict the deformed shape of the flexural robot, e.g., catheter, in real-time is a requirement. In this study, we have proposed and validated a fast and accurate model for flexural robots that has superior performance in computational time compared to the most accurate computational method in the literature, e.g., finite element method (FEM).

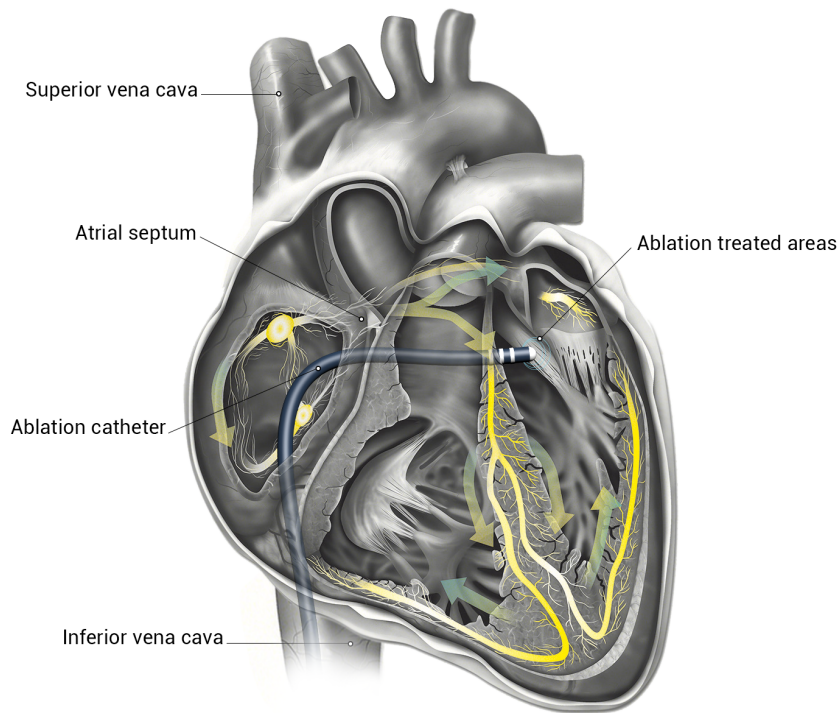


Figure 12: The schematic shape of steerable ablation catheters in the left atrium during ablation interventions.

3.1.2 Related Studies

From a mechanical point of view, flexural robots such as tendon-driven catheters, possess infinite degrees of freedom (DoF). Studies have mainly taken the discretization approach to reduce the number of DoFs on the flexural robots. Discretization would result in having a finite set of DoFs and would make the derivation of the equations of motion or balance equations easier [47]. However, reducing the DoFs would also result in the loss of information or erroneous deformation approximation. To avoid this source of error, studies have proposed to interpolate the deformation of the flexural robot using continuous shape interpolation functions, such as Bezier spline [93, 92]. Use of total or piecewise differentiable continuous curves result in differentiable deformation that can further be incorporated into the kinematics, balance, and constitutive equations [93, 52].

In this regard, Cardoso *et al.*[53] modeled a guidewire using a series of elastically connected vertices. The series of the vertices would model the backbone of a flexible catheter. Their model was fairly accurate for small deformations, i.e., deflection less than 15° , but would become erroneous at large deformations. Several methods for modeling large deflections of flexures have been proposed, e.g., elliptical integral approach [107], numerical integration approach with iterative shooting techniques [108, 109], incremental finite element or finite difference method with Newton–Raphson iteration techniques [110, 111, 112], and Cosserat rod model approach [113]. These approaches have been adopted in various studies on flexural robots. For example, Khoshnam *et al.*[71] used beam theory to simulate the distal portion of a catheter. On the other hand, traditional beam theories are not immediately applicable to large deflections. With deflection angles larger than $10 - 15^\circ$, the beam theory becomes erroneous. Furthermore, Cotin *et al.*[50] constructed an incremental finite element model based on beam theory, assuming the catheter is made up of wire-like segments.

Tunay *et al.*[114] developed an expanded model that included inflation, bending, twisting, extension, and shear deformation while reducing the total potential energy of the catheter locally. The most recent method adopted in the literature for flexural robots is the Cosserat rod model [115, 116]. Cosserat rod model results in a unified set of partial differential equations that govern both large and small deformations of the flexure. Nevertheless, the cosserat rod models are usually complex enough not to have analytical or fast-solving solution. To alleviate the aforementioned limitations for fast and accurate large deformation computation on flexural robots we have proposed a new method base on Bezier shape approximation and semi-analytical solution on a finite set of arcs along the flexure. The method is called finite arcs method (FAM) and was preliminarily tested for accuracy and speed and was compared to finite element analysis, as the most accurate method in the literature.

3.1.3 Contributions

The main contributions of this study are: 1) derivation of large deformation kinematics based on a finite number of arc segments with constant bending radius using Bezier shape interpolation of the arcs, 2) solution of large deformation of arc segments as a functional minimization problem, 3) validation of the proposed method for accuracy and speed for catheter deflection through comparison with simulation and experimental data.

In the following, first the derivation of the FAM model is presented and followed by the simulation and experiment-based validation.

3.2 Material and Methods

In this section, first, derivation of the kinematics, constitutive equation, and force balance equation for finding the deformation of a constant bending radius cantilever beam is provided. Afterwards, by aggregation of multiple segments the FAM problem is assembled and the total deformation is calculated.

3.2.1 Kinematics

The kinematics derivation of the catheter was based on a 3rd-order Bezier shape approximation that fulfilled a single-plane constant bending radius condition previously validated in [93]. Fig. 13 depicts the deformed shape of the catheter as a slender beam. In a previous study, the author showed that given the tip position of a circular arc in Γ -plane, i.e., (x, y) ,

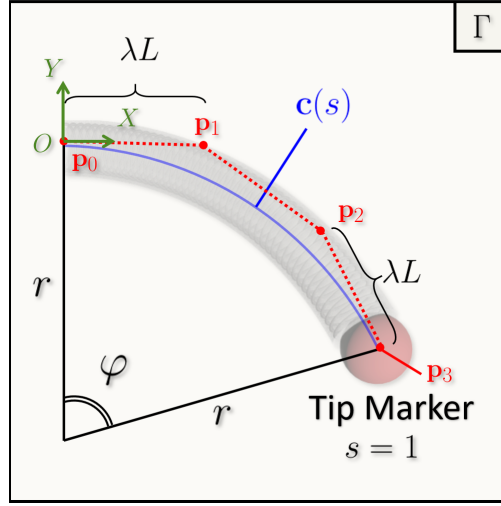


Figure 13: Schematic deformed shape of the tendon-driven continuum arm Bezier spline centerline. [93]

the shape of the catheter's centerline $\mathbf{c}(s)$ can be accurately approximated with:

$$\mathbf{c}(s) = \begin{pmatrix} x(s) \\ y(s) \\ z(s) \end{pmatrix} = \begin{pmatrix} \mathbf{p}_0 & \mathbf{p}_1 & \mathbf{p}_2 & \mathbf{p}_3 \end{pmatrix} \begin{pmatrix} (1-s)^3 \\ 3s(1-s)^2 \\ 3s^2(1-s) \\ s^3 \end{pmatrix}. \quad (7)$$

where, $s \in [0, 1]$ is the normalized length parameter, and $\mathbf{p}_i \in \Gamma$ are the control points determining the shape of $\mathbf{c}(s)$. The radius of curvature of the arm, r and bending angle φ were [117]:

$$r = \frac{x^2 + y^2}{2y}, \quad \varphi = \frac{L}{r} \quad (8)$$

and the control points in the Γ -plane would therefore have the coordinates:

$$\mathbf{p}_0 = \begin{pmatrix} 0 \\ 0 \\ 0 \end{pmatrix}, \mathbf{p}_1 = \lambda L \begin{pmatrix} 1 \\ 0 \\ 0 \end{pmatrix}, \mathbf{p}_2 = \begin{pmatrix} x \\ y \\ 0 \end{pmatrix} - \lambda L \begin{pmatrix} \cos \varphi \\ \sin \varphi \\ 0 \end{pmatrix}, \mathbf{p}_3 = \begin{pmatrix} x \\ y \\ 0 \end{pmatrix}, \quad (9)$$

with, x and y are the horizontal and vertical coordinates of the tip in the bending plane, Γ , and $\lambda \in [0, 1]$ is a constant controlling the curvature throughout shape [93]:

$$\lambda = \frac{1}{60(\cos \varphi - 1)} \times \left(- \left(4(1 - \cos \varphi) \left(\left(r - \frac{x}{2} \right)^2 - \frac{y^2}{4} \right) \times \right. \right. \\ \left. \left. \cos \varphi + y \left(r - \frac{x}{2} \right) \sin \varphi + r^2 + rx - \frac{x^2 + y^2}{4} \right) \right)^{\frac{1}{2}} - y \cos \varphi + \\ \left. (2r - x) \sin \varphi + y \right). \quad (10)$$

which is only a function of φ . From the geometry in Fig. 13 and the tip point could be parameterized in terms of φ as:

$$x = r \sin \varphi, \quad y = r(1 - \cos \varphi) \quad (11)$$

For the described single-plane bending of the catheter, the only kinematic variable was the geodesic bending curvature κ_g :

$$\kappa_g(s) = - \frac{x'(s)y''(s) - y'(s)x''(s)}{(x'^2(s) + y'^2(s))^{\frac{3}{2}}}, \quad (12)$$

with $(\cdot)' = \frac{d}{ds}(\cdot)$ as the derivation operator. For demonstration, Fig. 13 depicts circular arcs, their Bezier fittings, and their corresponding κ_g -s. As shown the proposed shape interpolation resulted in fair curvature approximations. However for bendings with $|\varphi| > \pi$, adopting an $n > 3$ would be necessary for accurate curvature approximation.

3.2.2 Constitutive Equation

The Euler-Bernoulli constitutive relationship between the bending deformation, i.e., $\kappa_g(s)$ – $\kappa_g^*(s)$, with $\kappa_g^*(s)$ as the initial curvature, and the internal moment, $\mathbf{m}(s)$ along the continuum arm was:

$$\mathbf{m}(s) = EI \begin{pmatrix} 0 \\ 0 \\ \kappa_g(s) - \kappa_g^*(s) \end{pmatrix}, \quad (13)$$

with EI as the flexural rigidity of the catheter. The constitutive equation implies that the internal bending moment has only an out-of-plane component perpendicular to Γ (in this case XY -plane). Also, by assuming the initial shape of the catheter as a straight line, $\kappa_g^*(s) = 0$ was assumed.

3.2.3 Moment Balance

For the sake of generality, it was assumed the catheter to bear an external force and an external moment at the tip. This loading is valid for tendon-driven catheters as a practical example. Fig. 14 shows the free-body diagram (FBD) of the catheter at equilibrium. The catheter is bent as a result of an external tip force \mathbf{f}^{Tip} and an external tip bending moment \mathbf{m}^{Tip} . In the case of tendon-driven catheter, the tip force and moment are results of the pulling in the catheter's steering tendons. Quasi-static equilibrium of the FBD depicted in Fig. 14 shows that the force and moment at the base of the catheter applied to it from its anchorage are:

$$\mathbf{f}_0 = -\mathbf{f}^{\text{Tip}}, \quad (14)$$

$$\mathbf{m}_0 = -\mathbf{m}^{\text{Tip}} - \begin{pmatrix} x \\ y \\ 0 \end{pmatrix} \times \mathbf{f}^{\text{Tip}}. \quad (15)$$

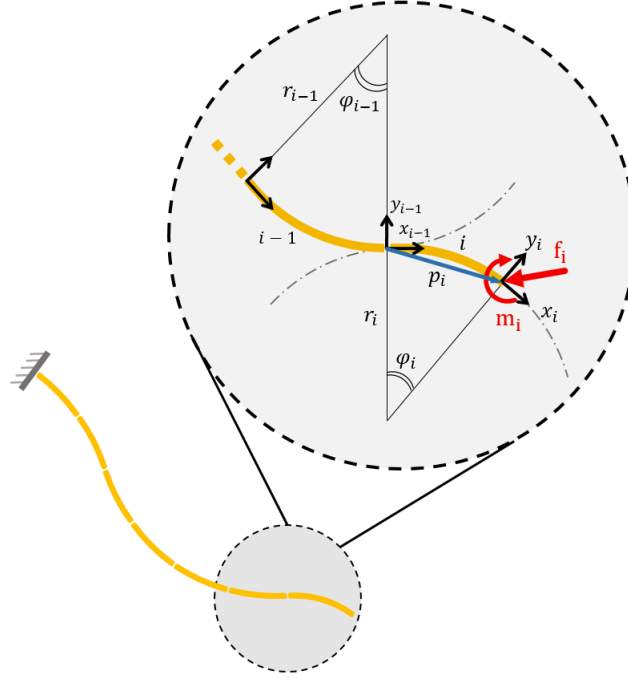


Figure 14: The free-body diagram (FBD) of a deformed catheter with multiple circular arc segments.

Also, the moment balance equation at any given point $\mathbf{p}(s) = \begin{pmatrix} x(s) & y(s) & 0 \end{pmatrix}^T$ throughout the catheter is:

$$\mathbf{m}(s) = \mathbf{m}^{\text{Tip}} + \begin{pmatrix} x - x(s) \\ y - y(s) \\ 0 \end{pmatrix} \times \mathbf{f}^{\text{Tip}}. \quad (16)$$

Substituting the constitutive definition of $\mathbf{m}(s)$ from Eq. 13, the balance equation, which relates the shape of the catheter to the tip force and moment, was obtained as:

$$\mathbf{m}^{\text{Tip}} + \begin{pmatrix} x - x(s) \\ y - y(s) \\ 0 \end{pmatrix} \times \mathbf{f}^{\text{Tip}} = EI \begin{pmatrix} 0 \\ 0 \\ \kappa_g(s) \end{pmatrix}. \quad (17)$$

This equation is a vectorial equation with two trivial scalar equations ($0 = 0$) from the first and second rows and a nonlinear bi-variable equation in terms of s and φ from the third

row:

$$m^{\text{Tip}} + f_y (x^{\text{Tip}}(\varphi) - x(s, \varphi)) - f_x (y^{\text{Tip}}(\varphi) - y(s, \varphi)) = \text{EI}\kappa_g(s, \varphi), \quad (18)$$

with m^{Tip} as the external tip moment applied through pulling the steering tendons, f_x and f_y as the horizontal and vertical components of the tip force in the bending angle, respectively. Also, the tip bending moment was known in real-time by measuring the torque of the driving motor. In this equation, the only unknown is the bending angle φ .

3.2.4 Deformation Solution

3.2.4.1 Solution for a single arc

As stated earlier, Eq. 18 is bi-variable in terms of s and φ . Since, the balance equation must be satisfied for all the points along the flexure's length, i.e., $s \in [0, 1]$, the balance equation was re-formulated as a functional minimization problem (Eq. 19) such that the integral of the squared residual error of the equation over $s \in [0, 1]$ would be minimized with an optimal φ . The solution of this minimization problem would result in the determination of φ that would determine the deformation the arc. The functional $\Pi(\varphi)$ was defined as:

$$\Pi(\varphi) = \int_0^1 \left(m^{\text{Tip}} + f_y (x(\varphi) - x(s, \varphi)) - f_x (y(\varphi) - y(s, \varphi)) - \text{EI}\kappa_g(s, \varphi) \right)^2 ds. \quad (19)$$

Functional $\Pi(\varphi)$ represents the summation of the residual of momentum balance equation along the length of the catheter. Minimization of $\Pi(\varphi)$, in fact, enforces Eq. 18 throughout the length of the flexure. The functional was further simplified to Eq. 21 by introducing:

$$\eta(s, \varphi) = m^{\text{Tip}} - \text{EI}\kappa_g(s, \varphi), \quad (20)$$

$$\Pi(\varphi) = \int_0^1 \left(f_y (x - x(s, \varphi)) - f_x (y - y(s, \varphi)) + \eta(s, \varphi) \right)^2 ds. \quad (21)$$

Given that the tip force was assumed to be applied by the driving tendons, and the fact that the tendons are tangent to the flexure's body, i.e., the tip force was assumed tangential to the deformed shape of the last segment. Thus, the functional Π simplified to:

$$\Pi(\varphi) = \int_0^1 \left(f_y \left(x - x(s, \varphi) + \tan \varphi (y - y(s, \varphi)) \right) + \eta(s, \varphi) \right)^2 ds. \quad (22)$$

Based on Eq. 8 and Eq. 11, x, y, r are functions of φ , thus the necessary condition for minimizing $\Pi(\varphi)$ was:

$$\frac{\partial}{\partial \varphi} \Pi(\varphi) = 0, \quad (23)$$

3.2.4.2 Generalization: multiple arcs (segments)

Based on the solution method provided above, it was hypothesized to discretize the flexure into N segments that each segment's deformation would be a single bending radius flexure. This way, the total deformation of the flexure would be obtained by summing all the deformations from the base $s = 0$ to the tip $s = 1$ of the flexure. Since the flexure would undergo large deformation, the internal moment and force at the boundaries of each segment would be obtained by translation and rotation of the forces on the segments next to it to the end points of the segment and then the deformation of the segment would be solved using Eq. 23. Thus, the deformation solution starts from the last segment and then propagates to the segments before it with transferring the internal moments and internal forces by knowing the deformation of the next segments. Fig. 14 depicts the proposed segmentation schematically. To the best of the author's knowledge, this approach is unprecedented in the literature. This angle for next section (φ_{i-1}) can be determined with the same process by transferring the resultant force and moment to section $i - 1$. For this transformation first the rotation matrix of i to $i - 1$ and translation matrix of end point in coordinate $i - 1$ are

as below:

$${}^{i-1}\mathbf{R}_i = \begin{pmatrix} \cos \varphi_i & -\sin \varphi_i & 0 \\ \sin \varphi_i & \cos \varphi_i & 0 \\ 0 & 0 & 1 \end{pmatrix} \quad (24)$$

$${}^{i-1}\mathbf{p}_i = \begin{pmatrix} x_i \\ y_i \\ z_i \end{pmatrix} = \begin{pmatrix} r_i \sin \varphi_i \\ r_i(1 - \cos \varphi_i) \\ 0 \end{pmatrix} \quad (25)$$

As a result, the amount of force and moment exerted on the endpoint of section $i - 1$ is obtained from the resultant force and moment from section i in addition to the external force and moment applied directly on section $i - 1$ which is formulated in Eq. 26 and 27.

$$\mathbf{F}_{i-1} = {}^{i-1}\mathbf{R}_i \mathbf{F}_i + \mathbf{F}_{i-1}^{ext} \quad (26)$$

$$\mathbf{m}_{i-1} = {}^{i-1}\mathbf{p}_i \times ({}^{i-1}\mathbf{R}_i \mathbf{F}_i) + \sum_{k=i}^N \mathbf{m}_k + \sum_{k=i}^N \mathbf{m}_k^{ext} \quad (27)$$

This process continues in a similar way to transmit force and momentum to all sections from the beam's free end to the base. In the end, the final deformed shape of the flexure was constructed by augmenting the deformed shape of segment $i + 1$ at the end of segment i . Eventually the deformed position of the end point of the n -th segment, \mathbf{P}_n in global coordination system was obtained as:

$$\mathbf{P}_n = \mathbf{P}_0 + \sum_{i=1}^n \mathbf{R} \left(\sum_{j=1}^i \varphi_j \right) \begin{pmatrix} \sin \varphi_i \\ (1 - \cos \varphi_i) \\ 0 \end{pmatrix} \frac{L_i}{\varphi_i}, \quad (28)$$

where \mathbf{P}_0 is the position of the base $s = 0$ of the flexure and L_i -s are the length of the i -th segment.

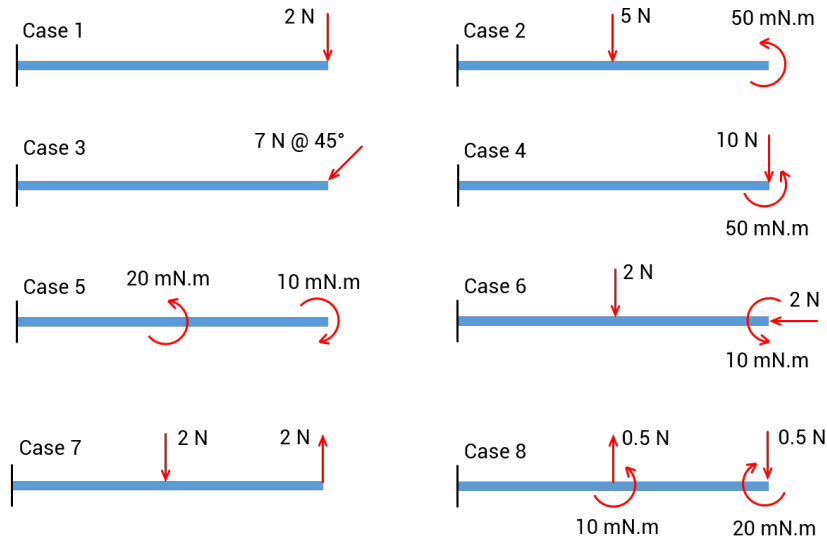


Figure 15: Eight load cases on a representative flexure for Study I.

3.3 Validation Studies

To assess the accuracy and computational performance of the proposed method, a simulation-based validation study and an experimental study were performed.

3.3.1 Study I: Simulation-based Validation

3.3.1.1 Simulation Protocol

To obtain the deformation of the RFA catheter in contact with atrial tissue, a planar FE model was developed and solved in Abaqus CAE 2020 student edition (Abaqus Inc., USA). Initially, the deformation of the steerable ablation catheter act as a cantilever beam simulated. Fig. 15 shows eight different load-cases in the simulation. The developed finite-element models of the catheter were similar to the prototyped 18-Fr catheter, i.e. 40×6 mm. Eight simulations with flexural rigidity of 750 Nmm^2 were performed.

Eq. 23 was derived analytically in Maple 2019 (Maplesoft, Cybernet Systems Co., Ltd.) and deformation calculation algorithm using Finite Arc Method (FAM) was developed

Table 1: Comparison of FAM and FEM solutions for eight load cases.

Case	Tip Displacement x^{Tip} (mm)			Tip Displacement y^{Tip} (mm)		
	FEM	FAM	Error	FEM	FAM	Error
1	11.35	11.53	-0.18	-31.55	-31.61	+0.06
2	33.51	33.16	+0.35	7.65	7.09	+0.56
3	28.17	29.67	-1.50	-15.83	-15.90	+0.07
4	-5.12	-6.38	+1.27	-7.79	-8.76	+0.97
5	39.53	39.26	+0.27	5.30	6.91	-1.60
6	36.84	37.42	-0.58	-14.21	-13.35	-0.86
7	33.96	34.11	-0.15	17.88	17.66	+0.22
8	32.53	33.81	-1.28	-18.98	-17.56	-1.41
Mean±SD	-	-	-0.27±0.90	-	-	-0.25±0.94

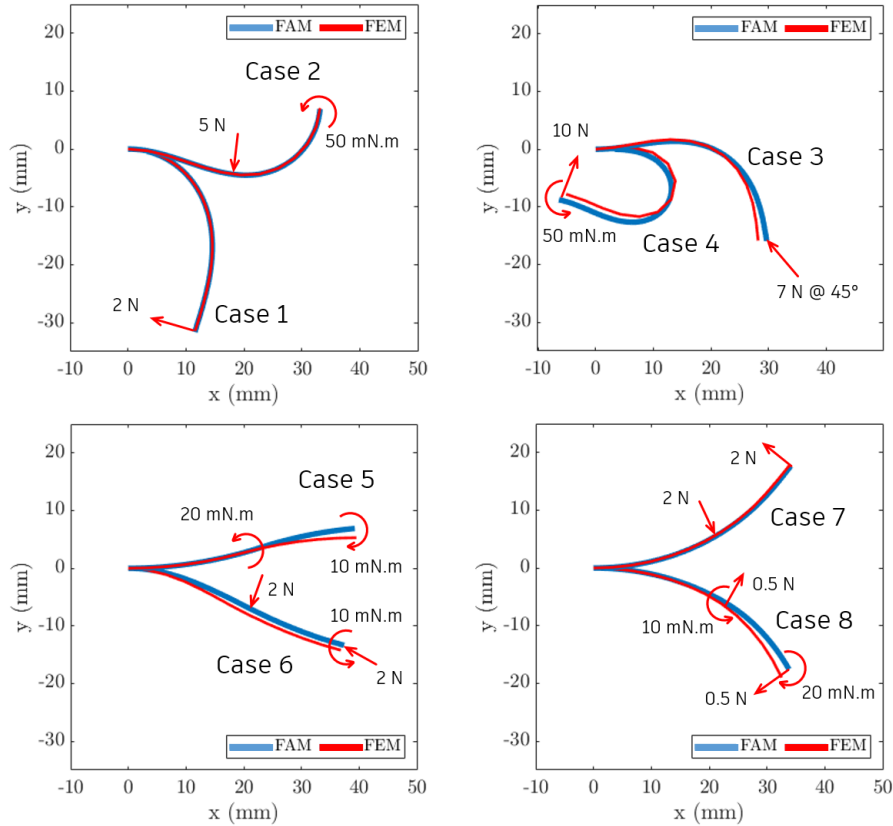


Figure 16: Comparison of FAM and FEM results in deflection estimations for eight load cases on soft flexures.

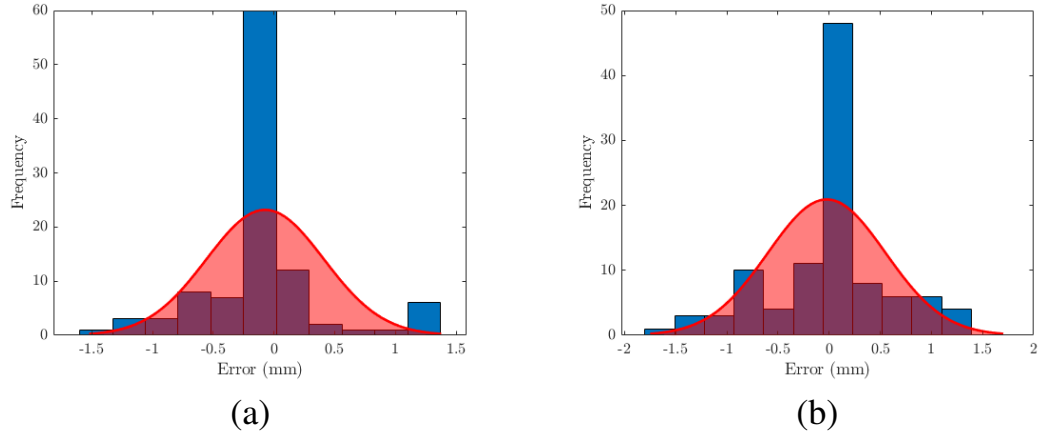


Figure 17: Distribution of error of deformation estimation with FEM as the reference along (a) x-direction and (b) y-direction.

in C++ programming language. The estimated deformation on each case was compared with the deformation originally solved in the simulation. The finite-element model of the catheter was constructed using quadratic `beam` elements with large deflection with 50 elements. The simulation results were not sensitive to mesh refinement for the number of elements used in the simulation. Also, the number of segments for the FAM solution was set to $N = 12$. The rationale for this selection and sensitivity of the results of FAM to the segmentation resolution are discussed in the results section.

3.3.1.2 Results

Fig. 16 shows the deformed shape of the catheters after applying force and moment in eight different cases (Fig. 15). In each load case, each segment was first λ was obtained using the proposed shape interpolation method (Eq. 10). Table 1 summarizes the results of the deformation simulation.

The comparison of the estimated tip position with the reference showed that the tip position estimation along x-axis had an average error of -0.27 ± 0.90 mm and along y-axis had an average error of -0.25 ± 0.94 mm.

The mean-absolute-error (MAE) of the deflection estimation with respect to the reference

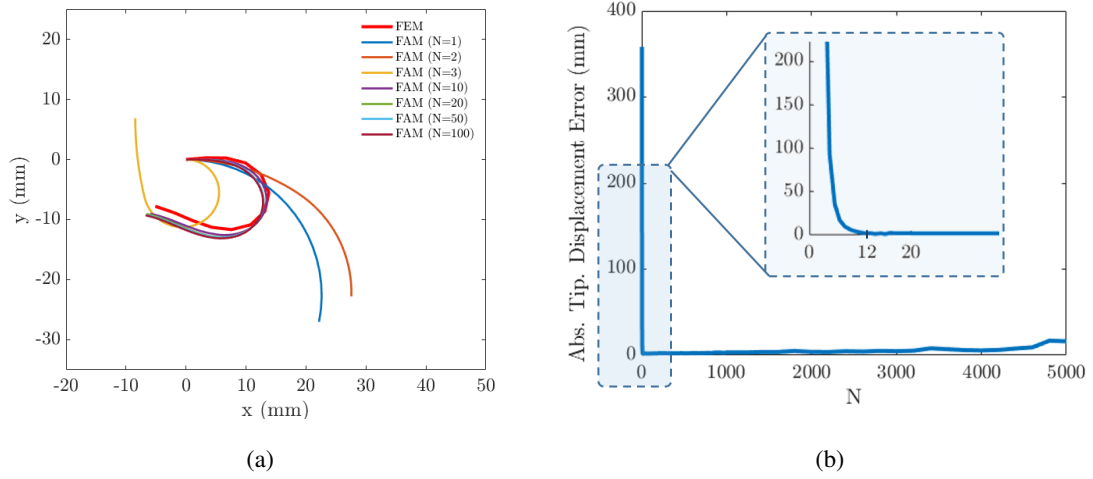


Figure 18: Effect of segmentation, (a) FAM deflection solution for different number of segments and (b) absolute tip displacement error for different number of segments.

was 0.29 ± 0.48 along x direction and 0.39 ± 0.58 along y direction with root-mean-square of 0.4865 and 0.5732 mm respectively (Fig. 17).

In order to investigate the segmentation effect, load case 4 was selected as the the worst-case-scenario and solved with a series of segmentation numbers. Fig. 18(a) shows a representative set of final shapes of the deformed catheter with various segmentation. The segmentation was changed between 1 to 5000 and the absolute error of the flexure’s tip position was studied (Fig. 18(b)). It was observed that by increasing the number of segments in the model from 1 the error dropped drastically and hit a minimum at 12 segments. The absolute error value was less than 3mm (7.5% of length) between $N=12$ and $N=500$. for $N>500$, the error increased incrementally until reaching to approximately 20mm (50% of length) at $N=5000$. Similar to finite element method, at extremely large number of segmentations the error increases due to the accumulation of round-off error. In addition, since for each segment a minimization problem is solved, at high number of segments, each segments becomes nearly a straight line and the residual error of the minimization increases as it cannot find a finite number for the curvature ($\varphi \rightarrow 0$).

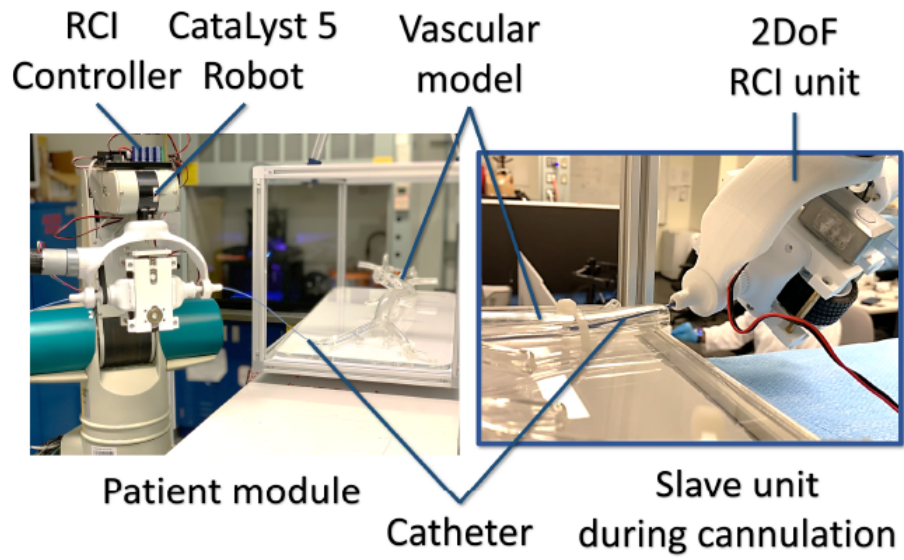
3.3.2 Study II: Experimental Validation

3.3.2.1 Setup and Protocol

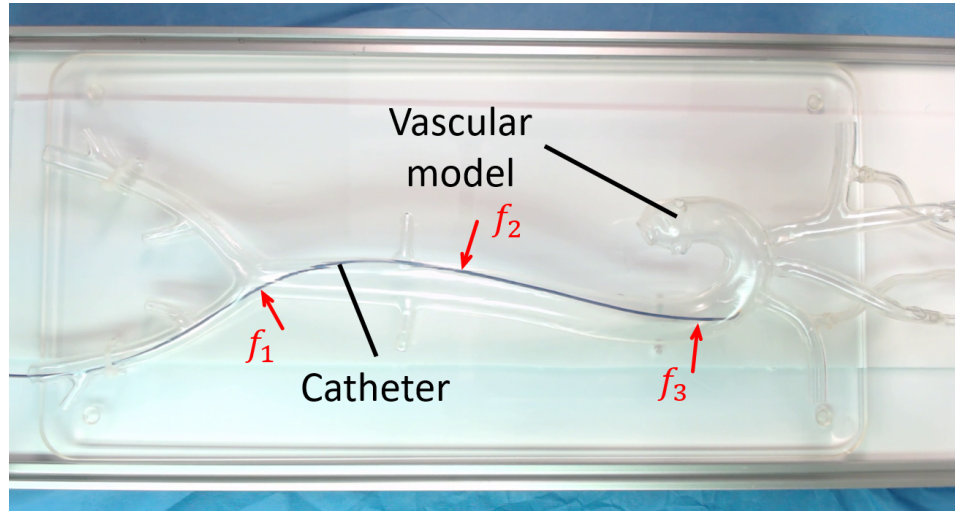
The proposed method was integrated with a representative robot-assisted intervention (RCI) system previously developed by the authors in [91, 77] to test the feasibility of integrating the proposed method with RCI systems (Fig. 19(a)). The user would transmit the measured rotation and insertion length to the patient module. As shown in Fig. 19(a), the CataLyst robot (Thermo Fisher, WA, USA) was used to align the entry angle of the femoral vein of the vascular model (SAM plus, Lake Forest Anatomical Inc., IL, USA). The forces and their location extracted using an image-based method developed by the authors in [77]. The total length of the catheter was 504 mm with hollow cylinder cross section with outer diameter of 2.14 and thickness of 0.29 mm. Its material is linear elastic with young's modulus of 1592.3 MPa and Poisson's ratio of 0.395 [77]. Three reaction forces were captured in the deformed shape of the catheters depicted in Fig. 19(b). The first force f_1 had a magnitude of $f_1 = 0.463N$ located at $s = 0.165$, the second force $f_2 = -0.065N$ was located at $s = 0.577$ and the third force was $f_3 = 0.007N$ located near the tip $s = 0.968$. The estimated forces from the deformed shape of the catheter were used in the FAM model of the catheter and the resultant deflections were compared.

3.3.2.2 Results

Fig. 20 compares the magnitude of the reference with the estimated deformation of catheter. As the comparison showed, the FAM results were in fair agreement with the observed deformation. The maximum absolute error of deflection along vertical axis y was 4.95 mm (8.5% of the maximum deflection), and it was at the tip. FAM method resulted in a larger estimation error at the tip which might be due to error accumulation through the segments



(a)



(b)

Figure 19: Setup used in validation study-II (a) patient module, (b) deflected catheter in the vascular model with the external forces.

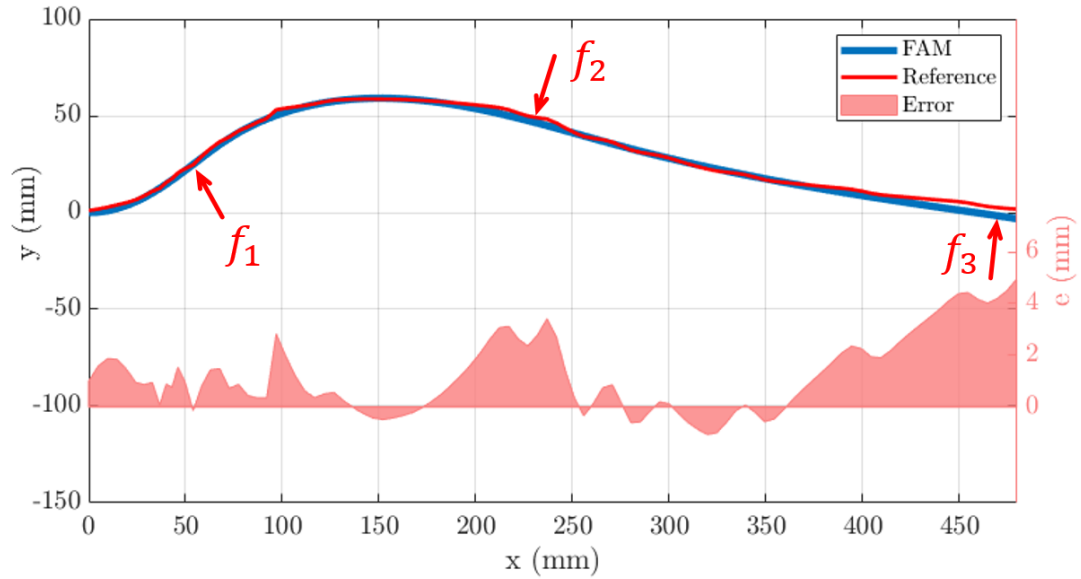


Figure 20: Comparison of FAM and ground truth deflections in Study II.

along the flexure. A similar trend was observed in Study I on the simulated deformation. Nevertheless, the average relative error of the experiments was 1.41 ± 1.47 mm. Another finding was that the average computational time of the proposed force estimation method was less than 3 ms, with C++ implementation. These findings showed that the proposed method could successfully simulate the deformation of flexures in realtime. The simulation-based and experimental validation studies showed the feasibility of the method and also the integrating of the proposed method with tendon-driven catheter actuation systems. Also, the validation studies showed acceptable accuracy of the proposed method in solving the deformation under varied conditions. Another extension of this work could be to use nonlinear constitutive equation and solution of the FAM thereof. The author have proposed such an integration with Cosserat rod models in [118]. The proposed method also can be used in sensor-based [46, 95, 119, 120] and sensor-free bending-based [92, 77] force estimation and haptic rendering [102, 121] for RCI systems.

3.4 Summary

In this chapter, a new modeling method and its solution for soft tendon-driven robots, i.e. catheters with large deformation using Finite Arc Method (FAM) was proposed and validated. The fast solution of the model solution was made possible by using the proposed Bezier spline shape approximation and discretizing the catheter into a finite set of circular arc segments. This study was a preliminary study to show the feasibility of the proposed method for planar deformations. Because of its planar assumptions, it might not be applicable to 3D deformations of catheters. Nevertheless, 3D deformations within a 3D surface can be modeled with the proposed method. The author have previously applied such an approach for single circular arc flexures in [56, 103].

Chapter 4

Impedance Matching Approach for Robust Force Feedback Rendering with Application in Robot-assisted Interventions

Robust and accurate force feedback is a clinical need for enhancing the safety of remote robot-assisted interventional procedures. In this study, an impedance-based force feedback approach was proposed and validated. Initially a fast impedance identification method for estimating the impedance of cathetervasculature interaction at the slave module of such systems was obtained. Afterward, a force feedback approach based on matching the mechanical impedance of the master module with the identified impedance was implemented. The proposed force control method was experimentally studied for a robotassisted remote catheter insertion task. Also, the performance of the proposed method was experimentally compared to the conventional direct force reflection approach. The proposed force feedback method exhibited fair accuracy in force tracking (meanabsolute error of 0.046 ± 0.027 N). The proposed method outperformed the direct force reflection approach in the absence and presence of communication interruptions (0.052N vs. 0.061N) and (0.041N vs. 0.171N), respectively. The proposed force feedback method exhibited favorable robustness and accuracy for remote interventional applications.

4.1 Background

robot-assisted cardiovascular intervention (RCI) systems have recently shown promising capabilities in enabling surgeons to perform long-distance cardiovascular interventions, e.g., tele-stenting [122] using 5G ultra-fast communications. This has expanded the scope of applications of the available RCI systems. Ultra-fast 5G networks are expected to show round-trip delays of as low as 1 ms [123], however, current remote RCI systems have faced communication delays of up to 163 ms in practice [122].

On the other hand, the lack of force feedback has been a limitation of the state-of-the-art robot-assisted cardiovascular intervention (RCI) systems [22]. This limitation may cause catastrophic outcomes by leading to irrecoverable tissue damage or vessel perforation [22]. Researchers have proposed using sensor-based [124] and sensorless [77, 56, 98] approaches to augment force feedback to the available RCI systems. With either approach, the force feedback system has an intrinsic rise-time to generate the desired force, typically around 100 ms.

The augmentation of force feedback to RCI systems is of even more importance when used in long-distance remote interventions. Whereas, in a local RCI procedure the surgeon is a few meters away from the patient and can switch the surgery to manual in case an adverse event happens; however, in the long-distance RCI scenario conversion to manual surgery is impossible; thus, it requires enhanced safety measures. Therefore, with the perspective of expanding long-distance RCI, having a robust and accurate force feedback for RCI systems is a pressing need which requires timely development.

Fig. 21 shows a conceptual representation of RCI systems with haptic feedback in remote intervention setup. The system has a slave-master configuration. The surgeons inserts/retracts and rotates a dummy catheter on the haptic interface of the master modules and her/his motion commands are transferred over a network communication channel to

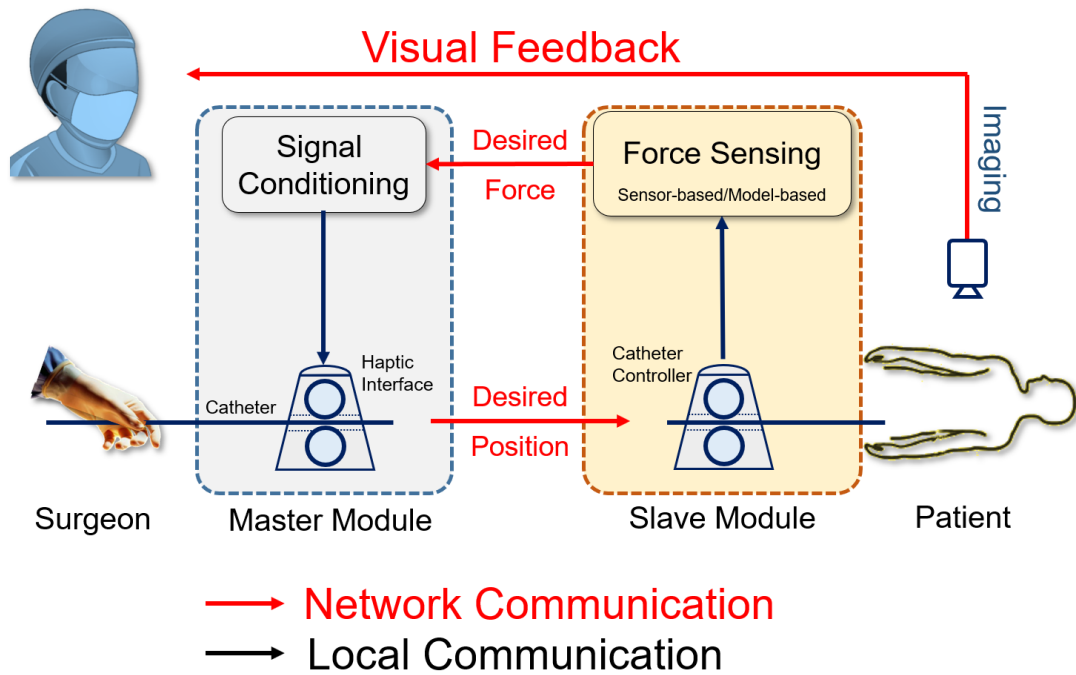


Figure 21: RCI system representation with DFR approach used for remote RCI procedures.

the catheter controller at the slave module. Simultaneously, the slave module controls the insertion depth and rotation of the medical catheter inside the patient's body according to the latest motion command received from the master module. Also, the surgeon receives real-time visual feedback from the images relayed from slave module [22].

In addition, the force sensing functionality at the slave module sends desired forces (measured/estimated at the slave) to the haptic interface of the master module. Similar to manual surgery, the surgeon would adapt the motion commands based on the visual and force feedbacks received.

Researchers have proposed different control methods for haptic feedback in remote surgery. Guo *et al.* utilized a direct force reflection (DFR) approach to track the desired force levels received from the slave module through DC-motor torque control and magnetic field control on magnetorheological fluidic haptic interfaces [125]. Although, DFR method

has shown acceptable performance for RCI application, it is dependent on receiving real-time updates from slave module for force tracking at a rate of up to 1 kHz. Sustaining such an update rate is necessary to maintain a robust force feedback in remote RCI. Given the network delay and disturbances associated with it, provision of accurate and robust force feedback is currently a technical challenge.

In this study, an impedance matching approach (IMA) for provision of force feedback in remote RCI is introduced as an alternative to the DFR. The main contributions of this study are: (1) proposing a force feedback control framework based on matching the impedance of master haptic interface to the slave exhibited impedance, (2) proposing a fast method for real-time identification of impedance at the slave module, and (3) experimental validation of the proposed force feedback method in the presence of substantial delay in the network communication. In the following, first the proposed framework for IMA, impedance identification method, and impedance control at the master module are described in Sec. 4.2. Afterwards, the design of study, experimental setup, and results of the validation studies are presented in Sec. 4.3. In the end, the concluding remarks and future studies are provided in 4.4.

4.2 Material and Method

4.2.1 Proposed Force Feedback Framework

Fig. 22 depicts the RCI system architecture with IMA-based force feedback proposed in this study. The main difference of the proposed framework with DFR approach (Fig. 21) is that the slave module would identify and relay the mechanical impedance of the catheter insertion, i.e. $\begin{pmatrix} m & c & k \end{pmatrix}^T$, instead of insertion (desired) force f_d . Locally in the master module, the desired force f_d for haptic interface would be estimated based on the desired trajectory $\begin{pmatrix} x_d & \dot{x}_d & \ddot{x}_d \end{pmatrix}^T$ from the haptic interface. Assuming the slave module tracks

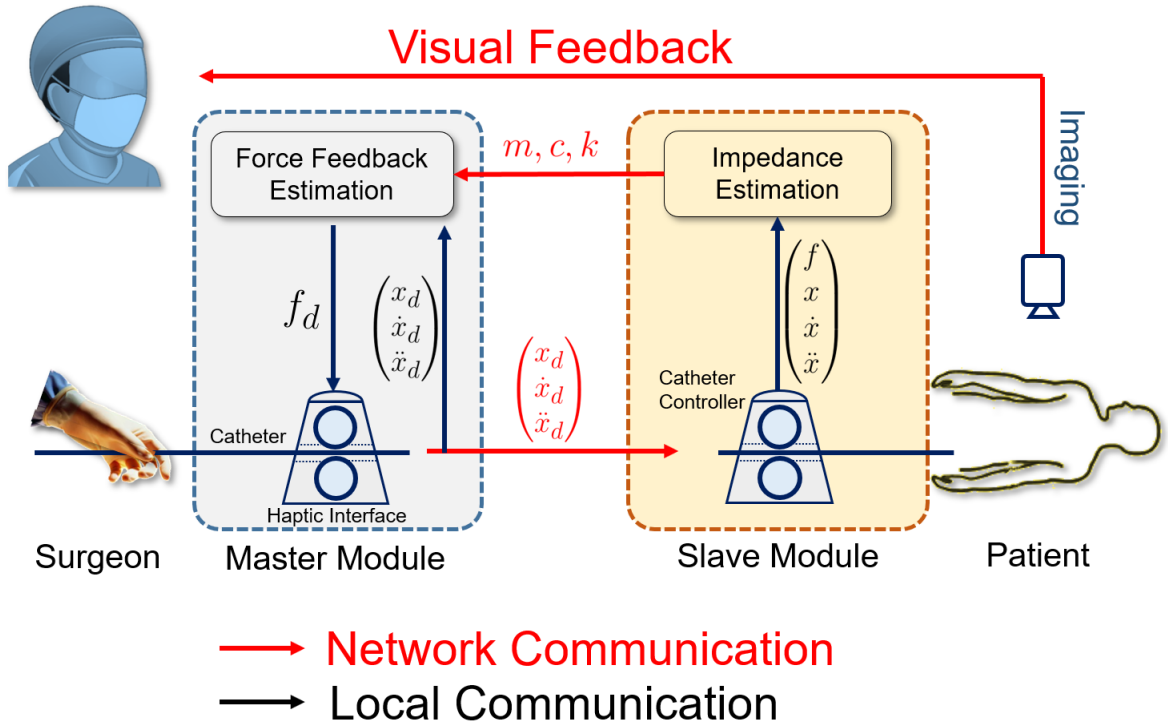


Figure 22: The proposed RCI system for remote RCI procedures with IMA-based force feedback.[22]

the desired trajectory with sufficient accuracy and since the mechanical impedance encodes the mechanical *behavior* of the catheter-patient interaction, it was hypothesized the IMA-based computed f_d would sufficiently resemble insertion force f at the slave module. The main implication of the IMA-based force feedback is that the desired force computation is immune to the connectivity delays and disturbances. In case the update of impedance from slave is delayed or corrupted (which is very common), the master module can still update f_d based on the latest impedance received from the slave module. Sharifi *et al.* showed that utilization of such a bi-lateral impedance matching for robotic cardiac surgery purposes would result in force conversion between the IMA computed force at master module and actual measured force at slave module [126].

4.2.2 Impedance Estimation at Slave Module

The force measured at the slave module is due to the interaction of the catheter and patient's vasculature [77]. Assuming the inserted catheter as the end-effector of the RCI robot at the patient side and adopting a linear impedance model [126], the insertion force of RCI was assumed to be of the form:

$$f = m\ddot{x} + c\dot{x} + kx, \quad (29)$$

where, m , c , and k represent the inertial, viscous, and elastic contribution coefficients of the catheter-vasculature interaction to the insertion force and $\begin{pmatrix} x & \dot{x} & \ddot{x} \end{pmatrix}^T$ are the state-variables. Typically, to estimate the impedance coefficients, a partial derivative of f with respect to the state-variables would be sufficient; however, such approach would reflect the instantaneous interaction of catheter and vasculature, the estimated impedance coefficients would change radically at consecutive time steps, and it is susceptible to derivation noises. It is noteworthy that unless a proper state-observer, e.g., Kalman filter, is used to track velocity and acceleration, these quantities may be of low signal-to-noise ratio.

Therefore and in order to obtain a robust impedance estimation schema, a fast optimization-based impedance identification method was adopted. To this end, a time window of width w was considered for time-history sampling of the state variables and insertion forces at slave. The time window would sweep over time as new data would become available at the slave. The width of the time window was selected as $w = 1000\text{ms}$ so that the impedance coefficients would represent the force-displacement behavior of the catheter-vasculature for the last 1 s at any instance during the surgery. To the best of the author's knowledge, time delays of more than 1 s have not been reported in the literature. At any instance of

time, the assembled force and state-variables in Eq. 29 would be of the form:

$$\begin{pmatrix} f_i \\ f_{i-1} \\ \vdots \\ f_{i-n} \end{pmatrix} = m \begin{pmatrix} \ddot{x}_i \\ \ddot{x}_{i-1} \\ \vdots \\ \ddot{x}_{i-n} \end{pmatrix} + c \begin{pmatrix} \dot{x}_i \\ \dot{x}_{i-1} \\ \vdots \\ \dot{x}_{i-n} \end{pmatrix} + k \begin{pmatrix} x_i \\ x_{i-1} \\ \vdots \\ x_{i-n} \end{pmatrix}, \quad (30)$$

where n was the number of samples collected during the last 1 s of the surgery and $i \in [0, n-1]$. Typically, the catheter trajectory control loop would run at a refresh-rate of 1kHz, thus, n would be in the order of 1000. For finding the optimized impedance coefficients, Eq. 30 was re-arranged:

$$\begin{pmatrix} f_i \\ f_{i-1} \\ \vdots \\ f_{i-n} \end{pmatrix} = \begin{pmatrix} \ddot{x}_i & \dot{x}_i & x_i \\ \ddot{x}_{i-1} & \dot{x}_{i-1} & x_{i-1} \\ \vdots & \vdots & \vdots \\ \ddot{x}_{i-n} & \dot{x}_{i-n} & x_{i-n} \end{pmatrix} \begin{pmatrix} m \\ c \\ k \end{pmatrix}, \quad (31)$$

which for better clarity can be expressed as:

$$\mathbf{f}_{n \times 1} = \mathbf{X}_{n \times 3} \tilde{\boldsymbol{\xi}}_{3 \times 1} \quad (32)$$

with \mathbf{f} and \mathbf{X} as knowns and $\tilde{\boldsymbol{\xi}}$ as unknown. Eq. 32 represents an over-constrained set of linear equations and constitutes a linear norm-minimization problem with respect to $\tilde{\boldsymbol{\xi}}$ such that:

$$\text{minimize } \left| (\mathbf{f} - \mathbf{X}\tilde{\boldsymbol{\xi}})^T (\mathbf{f} - \mathbf{X}\tilde{\boldsymbol{\xi}}) \right|. \quad (33)$$

Based on Moore-Penrose theorem in linear algebra, there exists necessarily a unique solution (Eq. 34) for the norm-minimization problem stated in Eq. 33.

$$\tilde{\boldsymbol{\xi}} = (\mathbf{X}^T \mathbf{X})^{-1} \mathbf{X}^T \mathbf{f}. \quad (34)$$

Since Eq. 34 merely involves matrix multiplications and $(\mathbf{X}^T \mathbf{X})$ is a 3×3 matrix, the computation of Eq. 34 is computationally fast. As will be discussed in Sec. 4.3, the computational time for Eq. 34 was less than 1 ms. It is noteworthy that since \mathbf{X} and \mathbf{f} vectors change incrementally with a first-in first-out sample collection sequence, the estimated impedance would not change abruptly during the procedure. This phenomenon is also observed in the experimental results.

4.2.3 Estimation of Force Feedback at Master Module

Assuming that the slave module tracks the error of catheter trajectory $\begin{pmatrix} x_d & \dot{x}_d & \ddot{x}_d \end{pmatrix}^T$ is negligible, the desired force feedback at master module was obtained using Eq. 35:

$$f_d = m\ddot{x}_d + c\dot{x}_d + kx_d. \quad (35)$$

Since the estimated impedance coefficients would not change abruptly during the procedure, the desired force also would not experience radical jumps.

4.2.4 Comparison of PID Controller with IMA Controller

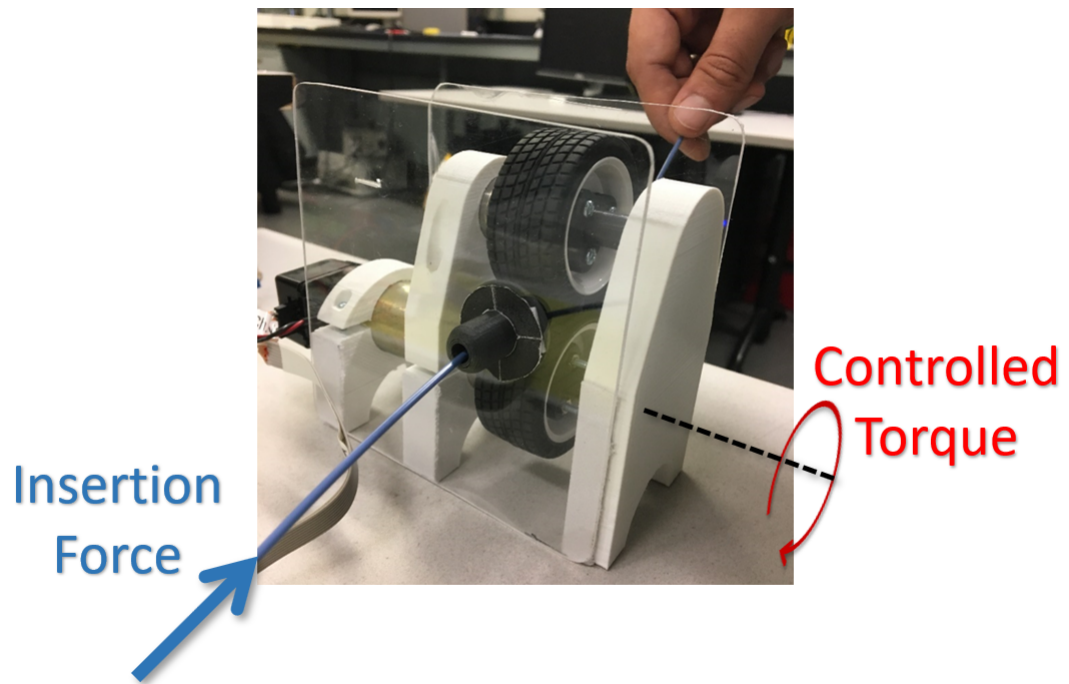
Eq. 36 expresses the PID controller rule which is used to control the force on RCI systems.

$$i = k_p e + k_d \frac{de}{dt} + k_i \int_0^t e dt \quad \text{with } e = f_m - f_d \quad (36)$$

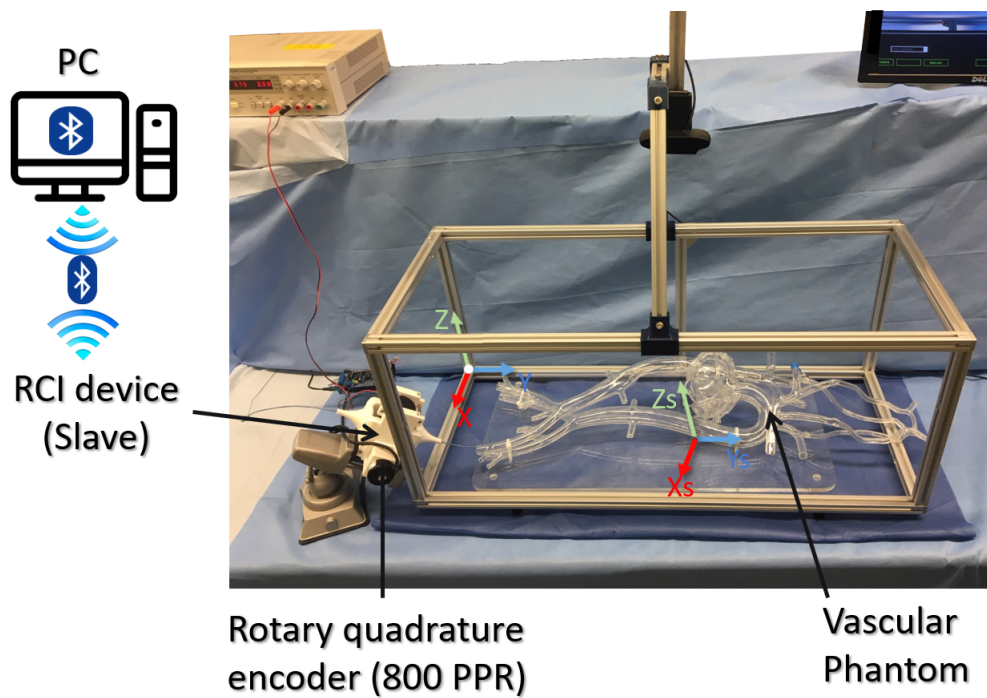
where, k_p , k_d , and k_i are the proportional, derivative, and integral coefficients of the PID tuning its tracking performance while e , f_m , and i are the force tracking error, the force measured at the haptic interface of the master module, and the electrical current provided to the DC-motor of the haptic interface. From Eq. 36 it is observed that the PID controller would try to keep the tracking error e at zero. If an interruption in the update of f_d happens during RCI procedure, PID would maintain the force feedback at the latest desired force received from the slave. This behavior would result in high tracking error with respect to the actual forces measured at the slave. Also, once the stream of data from slave resumes after interruption, the setpoint of PID may experience abrupt change (due to changes in the interaction forces) and might result in abrupt jump in the current of motor (Eq. 36). Nevertheless, in case of an communication interruption, the proposed IMA would continuously use the latest ($\tilde{\xi}$) Eq. 35 to update f_d .

4.3 Validation Studies

The experimental validation of this study was performed using the available setup developed by Hooshiar *et al.* [77]. The master module of the utilized RCI system (Fig. 23(a)) was equipped with a DC-motor, a quadrature encoder, and motor control module (Phidgets Inc., Calgary, Canada). The master module was capable of measuring the catheter insertion trajectory $\begin{pmatrix} x_d & \dot{x}_d & \ddot{x}_d \end{pmatrix}^T$ and providing force-feedback through closed-loop current control of the DC-motor. The slave module Fig. 23(b) was similar to the master module and was used to cannulate a clinical Runway Guide Catheter (Boston Scientific Corp., MA, USA) into a phantom vascular model (SAM Plus, Lake Forest Anatomical, IL, USA). The slave module was capable of tracking the catheter insertion trajectory with less than 5% tracking error [77]. For the comparison purposes, the reference insertion force (reference desired force) was recorded at a sampling rate of 1 kHz using an ATI Mini force-torque sensor (ATI Industrial Automation Inc., NC, USA) installed below the vascular phantom measuring the



(a)



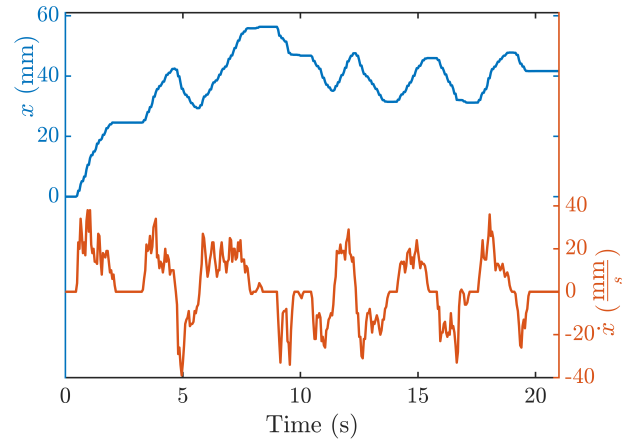
(b)

Figure 23: RCI device used in the experiments: (a) master, (b) slave module.

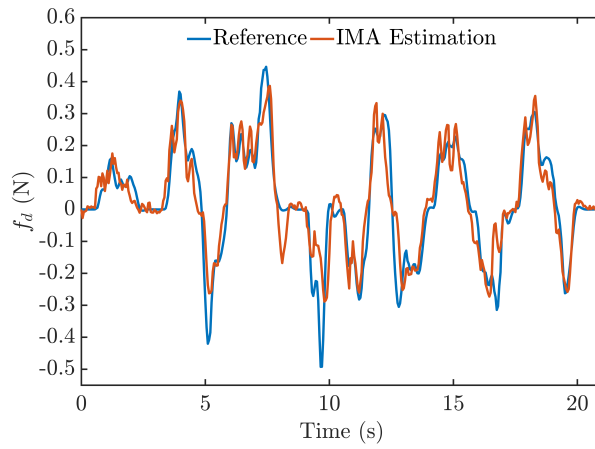
total insertion force. The control logic for both PID and IMA controllers were implemented in hardware-software-integrated architecture using C# programming language. The master-slave connectivity was established using a universal data protocol (UDP) on a local intranet network with an added latency of 200 ms (to simulate the communication delay reported in the literature [122]). The post-processing of the data was performed in Matlab 2019Rb (Mathworks Inc., MA, USA).

4.3.1 Experiment I: Impedance Estimation at Slave Module

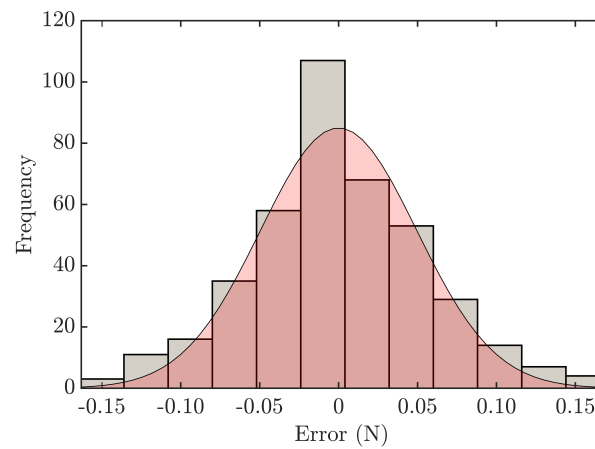
Fig. 24(a) shows the insertion length of the velocity of the catheter recorded at the slave module. In Experiment I, the catheter was arbitrarily inserted/retracted. The maximum insertion length was 56 mm and the maximum insertion velocity was $41.3 \frac{\text{mm}}{\text{s}}$. During the test, the impedance of catheter insertion at the slave was calculated using Eq. 34 with $w = 1 \text{ s}$, and was relayed to the master module over UDP channel. The average impedance computation time at the slave module was $0.32 \pm 0.17 \text{ ms}$. This computation time corresponds to a (minimum) refresh rate 2040 Hz which is above the maximum refresh rate of the force control loop ($\approx 1000 \text{ Hz}$). The haptic interface of the master module controlled the force inserted to the hand of the operator using its internal current-control loop to track the IMA-based force estimation. Fig. 24(b) compares the force applied to the hand of the operator (output of the master haptic interface) with the reference force measured at the slave. The results shows a fair force tracking performance for the proposed IMA-based force feedback. The maximum insertion force was 0.387 N and the mean-absolute-error (MEA) of force tracking error was $0.046 \pm 0.027 \text{ N}$ ($\approx 11\%$ of maximum force). The distribution of the tracking error (Fig. 24(c)) showed a normal distribution.



(a)



(b)



(c)

Figure 24: (a) Inserted length and velocity of the catheter in Experiment I, (b) tracking performance of IMA, and (c) distribution of force tracking error.

4.3.2 Experiment II: Comparison of DFR and IMA with Communication Interruption

In order to compare the robustness of the proposed IMA method with PID-based DFR for force feedback, two separate tests were performed. In the first test, the master force feedback was rendered through DFR approach by merely relaying the latest received f_d from the slave to the haptic interface force controller. In the second test, the impedance information from the slave was relayed to the IMA force estimator at the master module and f_d was temporally regulated according to the latest received $\tilde{\xi}$. In both tests, the UDP communication from master to slave was stopped for 1 s at $t = 4$ s and $t = 8$ s.

Fig 25(a) shows the force feedback tracking of PID-based DFR approach. It was observed that in the absence of network delay, DFR fairly followed the reference (desired) force (MAE= 0.061 ± 0.034 N). However, once f_d update is stopped at $t = 4$ s and $t = 8$ s, PID fails to follow the reference force (MAE= 0.171 ± 0.114 N) and maintains the latest f_d level received from the slave module. Also, once the f_d update resumes at $t = 5$ s and $t = 9$ s, PID abruptly increases the force to track the updated f_d . Such an abrupt change in the force, if the dummy catheter is not firmly grasped by the surgeon, may result in catheter slippage and lead to system instability. Since the motion commands are simultaneously relayed to the slave module, such catheter slippage (instabilities) may cause unwanted motion at the catheter inside the patient body and cause irreversible damage.

Fig. 25(b), shows the performance of IMA force feedback controller during the second test. It was observed that the IMA force controller has successfully followed the reference force both during normal communication with the slave (MAE= 0.052 ± 0.042) and while $\tilde{\xi}$ was not updated (disrupted communication) (MAE= 0.041 ± 0.033). Also, Fig. 25(c) shows the changes in impedance coefficients, m , c , k . As expected, the values of impedance coefficients did not change while the communication channel with the slave module was stopped,

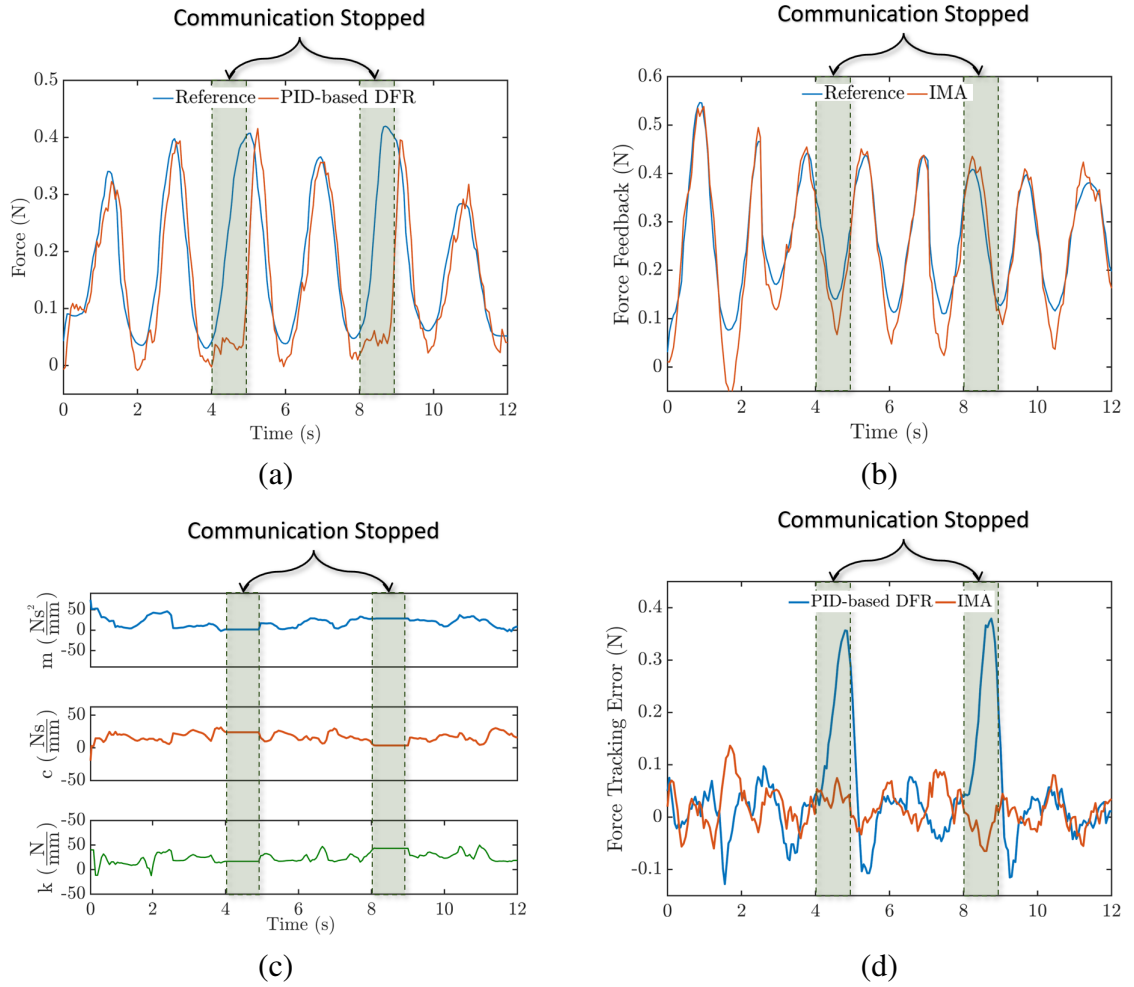


Figure 25: (a) Force tracking performance of PID-based DFR, (b) force tracking performance of IMA controller, (c) temporal changes in impedance coefficients used by IMA, and (d) comparison of the force tracking error with PID-based DFR and IMA controller.

i.e. shaded area in Fig. 25. Fig. 25(d) compares the force tracking errors of PID and IMA controllers. As depicted, the force tracking error of PID controller was larger than IMA controller, especially during the communication stoppage. The maximum tracking error for PID controller was 0.374 N while it was 0.074 N for IMA controller. The IMA controller outperformed the DFR controller both with and without communication disruption. This experiment showed the validity of the hypothesis of this study. The IMA outperforms DFR due to the fact that the proposed IMA controller in fact uses the latest impedance information to predict the force feedback based on the catheter trajectory obtained from master while the FDR controller stagnates at the latest f_d received from the slave module.

4.4 Summary

In this study, initially an impedance-based force feedback controller was proposed, implemented, and its performance was experimentally studied. Afterward, the performance of the proposed controller was compared to the conventional PID-based DFR for force feedback tracking task in an RCI mock procedure. The proposed controller outperformed the DFR controller in accuracy and robustness both during uninterrupted and interrupted network communications. The advantage of using IMA force feedback strategy relies on the fact that IMA conveys encoded information about the mechanical *behavior* of the catheter-vasculature interaction while DFR merely relies on obtaining its desired force from the slave. Given that RCI procedures are intrinsically risky procedures, IMA would make a superior choice for augmentation of force feedback to the state-of-the-art RCI systems. For future studies, the author will incorporate a nonlinear impedance identification to the framework with temporal linearization for more accurate IMA force estimation. Also, a learn-from-history method for adapting the impedance coefficient during interrupted communication will be incorporated.

Chapter 5

Conclusions and Future Works

5.1 Conclusions

This research was aimed at addressing the clinical need for robust, fast, and accurate haptic rendering during robot-assisted cardiovascular intervention procedures. To this end, first the clinical requirements of accuracy and speed pertinent to haptic rendering were extracted from the literature. Afterwards, three independent studies were performed that contributed to improvement of the state-of-the-art of various components of RCI systems.

More specifically, the objective of this thesis was to develop, verify, and validate mechatronics technology for real-time accurate and robust haptic feedback rendering for RCI systems. The design requirements based on the clinical requirements were 1) using total tip contact force as the haptic cue with an operational range of 0–2 N, with an error of less than 10% of full-scale, and a minimum refresh rate of 25 Hz.

To this end, by considering the need to avoid adding an additional technology-related step to the surgical workflow, a new learning-based force estimation framework for steerable catheters based on the learning-from-simulation principle was proposed and validated in Chapter 3. The utilization of a Bezier shape fitting method facilitated the reduction of

input space dimensions for the models. Afterwards, the trained models were used in an ex-vivo validation study for real-time image-based force estimation on a commercial ablation catheter. The adopted nonlinear regression models, i.e., ANN and SVR were of acceptable accuracy within the clinical requirements range, i.e., error less than 10% of full-scale.

In continuation, a new modeling method and its solution for soft tendon-driven robots with large deformation using Finite Arc Method (FAM) was proposed and validated in Chapter 3. The fast solution of the model was made possible by using a Bezier spline shape approximation and discretizing the catheter into a finite set of circular arc segments.

In Chapter 4, the aim was to rely on the estimated contact force at the patient module (follower) to the leader robot (leader). In practice, the estimated tip contact force at the follower could be estimated using the proposed learning-based-model in Chapter 2. In order to achieve this objective, a novel impedance-based force feedback rendering modality was proposed and implemented on a representative teleoperated RCI system for experimental validation. To this end, initially an impedance-based force feedback controller was proposed, implemented, and its performance was experimentally studied. Afterwards, the performance of the proposed controller was compared to the conventional PID-based DFR for force feedback tracking task in an RCI mock procedure. The proposed controller outperformed the DFR controller in accuracy and robustness both during uninterrupted and interrupted network communications, and it showed compatibility with the design requirements as a feasible technology to address the need for the provision of haptic feedback for RCI systems.

In conclusion, the studies performed in this research showed the feasibility of fast, accurate, and robust image-based tip force estimation and haptic rendering for teleoperated RCI systems with compliance to the clinical requirements.

5.2 Future Works

To improve the studies of this research in future works:

- (1) The method studied in chapter 3 was the planar deflection of the catheter that may not always be valid in real surgical applications. However, the proposed shape interpolation method and the learning model architectures thereof allow for 3D shape interpolation and force estimation. In future studies, use of stereo-vision for 3D shape acquisition can contribute to the alleviation of this limitation.
- (2) Similarly, the planar deflection assumption for the catheter in Chapter 2 might not always be valid. In future studies, parameteric spatial deformation estimation especially with an extended spatial FAM model could be investigated.
- (3) Replacement of the FE simulation with a less computationally costly method such as Cosserat rod modeling and direct incorporation of the Bezier shape interpolation with the model formulation, such as proposed in [98], may facilitate generation of larger training dataset for the inclusion of 3D load-cases.
- (4) Researchers can incorporate a nonlinear impedance identification to the framework with temporal linearization for more accurate IMA force estimation.
- (5) Also, a learn-from-history method for adapting the impedance coefficient during interrupted communication can be incorporated.

Bibliography

- [1] Kanu Chatterjee. *Cardiologyan illustrated textreference*. 1991.
- [2] Philip J Podrid and Robert J Myerburg. Epidemiology and stratification of risk for sudden cardiac death. *Clinical Cardiology: An International Indexed and Peer-Reviewed Journal for Advances in the Treatment of Cardiovascular Disease*, 28(S1):3–11, 2005.
- [3] Alan S Go, Elaine M Hylek, Kathleen A Phillips, YuChiao Chang, Lori E Henault, Joe V Selby, and Daniel E Singer. Prevalence of diagnosed atrial fibrillation in adults: national implications for rhythm management and stroke prevention: the anticoagulation and risk factors in atrial fibrillation (atria) study. *Jama*, 285(18):2370–2375, 2001.
- [4] Simon Stewart, Carole L Hart, David J Hole, and John JV McMurray. A population-based study of the long-term risks associated with atrial fibrillation: 20-year follow-up of the renfrew/paisley study. *The American journal of medicine*, 113(5):359–364, 2002.
- [5] Charles Florin, Nikos Paragios, and Jim Williams. Particle filters, a quasi-monte carlo solution for segmentation of coronaries. In *International conference on medical image computing and computer-assisted intervention*, pages 246–253. Springer, 2005.
- [6] Susan Colilla, Ann Crow, William Petkun, Daniel E Singer, Teresa Simon, and Xi-anchen Liu. Estimates of current and future incidence and prevalence of atrial fibrillation in the us adult population. *The American journal of cardiology*, 112(8):1142–1147, 2013.
- [7] Rashid Ghorbani Afkhani, Ghanbar Azarnia, and Mohammad Ali Tinati. Cardiac arrhythmia classification using statistical and mixture modeling features of ecg signals. *Pattern Recognition Letters*, 70:45–51, 2016.
- [8] Peter J Mohler, Igor Splawski, Carlo Napolitano, Georgia Bottelli, Leah Sharpe, Katherine Timothy, Silvia G Priori, Mark T Keating, and Vann Bennett. A cardiac arrhythmia syndrome caused by loss of ankyrin-b function. *Proceedings of the National Academy of Sciences*, 101(24):9137–9142, 2004.

- [9] Arthur AM Wilde and Connie R Bezzina. Genetics of cardiac arrhythmias. *Heart*, 91(10):1352–1358, 2005.
- [10] Xiu-Shan Wu, Wanwan Cai, Ping Zhu, and Wuzhou Yuan. New strategies for arrhythmia treatment. *Journal of Cardiology and Therapy*, 5(1):756–763, 2018.
- [11] Ahmed AlTurki, Riccardo Proietti, Vincenzo Russo, Tarvinder Dhanjal, Prithwish Banerjee, and Vidal Essebag. Anti-arrhythmic drug therapy in implantable cardioverter-defibrillator recipients. *Pharmacological research*, 143:133–142, 2019.
- [12] Ian D McRury and David E Haines. Ablation for the treatment of arrhythmias. *Proceedings of the IEEE*, 84(3):404–416, 1996.
- [13] ROY Beinart, Suhny Abbara, Andrew Blum, Maros Ferencik, Kevin Heist, Jeremy Ruskin, and Moussa Mansour. Left atrial wall thickness variability measured by ct scans in patients undergoing pulmonary vein isolation. *Journal of cardiovascular electrophysiology*, 22(11):1232–1236, 2011.
- [14] Burr Hall, Vinodh Jeevanantham, Rochelle Simon, John Filippone, Gabriel Vorobiof, and James Daubert. Variation in left atrial transmural wall thickness at sites commonly targeted for ablation of atrial fibrillation. *Journal of Interventional Cardiac Electrophysiology*, 17(2):127–132, 2006.
- [15] Martin Bishop, Ronak Rajani, Gernot Plank, Nicholas Gaddum, Gerry Carr-White, Matt Wright, Mark O’Neill, and Steven Niederer. Three-dimensional atrial wall thickness maps to inform catheter ablation procedures for atrial fibrillation. *Europace*, 18(3):376–383, 2016.
- [16] Abhishek Bhaskaran, William Chik, Jim Pouliopoulos, Chrishan Nalliah, Pierre Qian, Tony Barry, Fazlur Nadri, Rahul Samanta, Ying Tran, Stuart Thomas, et al. Five seconds of 50–60 w radio frequency atrial ablations were transmural and safe: an in vitro mechanistic assessment and force-controlled in vivo validation. *Europace*, 19(5):874–880, 2017.
- [17] Yusof Ganji, Farrokh Janabi-Sharifi, et al. Catheter kinematics for intracardiac navigation. *IEEE Transactions on Biomedical Engineering*, 56(3):621–632, 2009.
- [18] Dipen C Shah, Hendrik Lambert, Hiroshi Nakagawa, Arne Langenkamp, Nicolas Aeby, and Giovanni Leo. Area under the real-time contact force curve (force–time integral) predicts radiofrequency lesion size in an in vitro contractile model. *Journal of cardiovascular electrophysiology*, 21(9):1038–1043, 2010.
- [19] Dingfei Ge, Narayanan Srinivasan, and Shankar M Krishnan. Cardiac arrhythmia classification using autoregressive modeling. *Biomedical engineering online*, 1(1):1–12, 2002.

- [20] Giora Weisz, D Christopher Metzger, Ronald P Caputo, Juan A Delgado, J Jeffrey Marshall, George W Vetrovec, Mark Reisman, Ron Waksman, Juan F Granada, Victor Novack, et al. Safety and feasibility of robotic percutaneous coronary intervention: Precise (percutaneous robotically-enhanced coronary intervention) study. *Journal of the American College of Cardiology*, 61(15):1596–1600, 2013.
- [21] Nathaniel R Smilowitz, Jeffrey W Moses, Fernando A Sosa, Benjamin Lerman, Yasir Qureshi, Kate E Dalton, Lauren T Privitera, Diane Canone-Weber, Varinder Singh, Martin B Leon, et al. Robotic-enhanced pci compared to the traditional manual approach. *J Invasive Cardiol*, 26(7):318–321, 2014.
- [22] Amir Hooshidar, Siamak Najarian, and Javad Dargahi. Haptic telerobotic cardiovascular intervention: a review of approaches, methods, and future perspectives. *IEEE Reviews in Biomedical Engineering*, 13:32–50, 2020.
- [23] Hedyeh Rafii-Tari, Christopher J Payne, Colin Bicknell, Ka-Wai Kwok, Nicholas JW Cheshire, Celia Riga, and Guang-Zhong Yang. Objective assessment of endovascular navigation skills with force sensing. *Annals of biomedical engineering*, 45(5):1315–1327, 2017.
- [24] Simon K Neequaye, Rajesh Aggarwal, Isabelle Van Herzeele, Ara Darzi, and Nicholas J Cheshire. Endovascular skills training and assessment. *Journal of vascular surgery*, 46(5):1055–1064, 2007.
- [25] Timothy R Coles, Dwight Meglan, and Nigel W John. The role of haptics in medical training simulators: A survey of the state of the art. *IEEE Transactions on haptics*, 4(1):51–66, 2010.
- [26] Baofeng Gao, Shuxiang Guo, Nan Xiao, and Jin Guo. Design of the virtual reality based robotic catheter system for minimally invasive surgery training. In *2012 IEEE International Conference on Automation and Logistics*, pages 611–616. IEEE, 2012.
- [27] Klaus A Hausegger, Peter Schedlbauer, Hannes A Deutschmann, and Kurt Tiesenhäusen. Complications in endoluminal repair of abdominal aortic aneurysms. *European journal of radiology*, 39(1):22–33, 2001.
- [28] Tsuyoshi Kaneko and Walter Randolph Chitwood Jr. Current readings: Status of robotic cardiac surgery. In *Seminars in thoracic and cardiovascular surgery*, volume 25, pages 165–170. Elsevier, 2013.
- [29] Ryan Madder, Paul Campbell, Ehtisham Mahmud, David Wohns, Tomasz Stys, Ronald Caputo, Mark Leimbach, Manish Parikh, Vijaykumar Kasi, and Giora Weisz. Multi-center post-market registry for the evaluation of robotic assisted pci. *Journal of the American College of Cardiology*, 67(13S):224–224, 2016.
- [30] Yasuo Okumura, Susan B Johnson, T Jared Bunch, Benhur D Henz, CHRISTINE J O’BRIEN, and Douglas L Packer. A systematical analysis of in vivo contact forces

- on virtual catheter tip/tissue surface contact during cardiac mapping and intervention. *Journal of cardiovascular electrophysiology*, 19(6):632–640, 2008.
- [31] Hardik J Pandya, Jun Sheng, and Jaydev P Desai. MemS-based flexible force sensor for tri-axial catheter contact force measurement. *Journal of microelectromechanical systems*, 26(1):264–272, 2016.
- [32] R Surapaneni, Q Guo, Y Xie, DJ Young, and CH Mastrangelo. A three-axis high-resolution capacitive tactile imager system based on floating comb electrodes. *Journal of Micromechanics and Microengineering*, 23(7):075004, 2013.
- [33] Pietro Valdastri, Keith Houston, Arianna Menciassi, Paolo Dario, Arne Sieber, Masaru Yanagihara, and Masakatsu Fujie. Miniaturised cutting tool with triaxial force sensing capabilities for minimally invasive surgery. In *Engineering Systems Design and Analysis*, volume 42495, pages 517–524, 2006.
- [34] Javad Dargahi, Saeed Sokhanvar, Siamak Najarian, and Siamak Arbatani. *Tactile sensing and displays: haptic feedback for minimally invasive surgery and robotics*. John Wiley & Sons, 2012.
- [35] Caroline Medi, Lisbeth Evered, Brendan Silbert, Andrew Teh, Karen Halloran, Joseph Morton, Peter Kistler, and Jonathan Kalman. Subtle post-procedural cognitive dysfunction after atrial fibrillation ablation. *Journal of the American College of Cardiology*, 62(6):531–539, 2013.
- [36] Graham Robinson and J Bruce C Davies. Continuum robots—a state of the art. In *Proceedings 1999 IEEE international conference on robotics and automation (Cat. No. 99CH36288C)*, volume 4, pages 2849–2854. IEEE, 1999.
- [37] Yoshihiko Nakamura, Kousuke Kishi, and Hiro Kawakami. Heartbeat synchronization for robotic cardiac surgery. In *Proceedings 2001 ICRA. IEEE International Conference on Robotics and Automation (Cat. No. 01CH37164)*, volume 2, pages 2014–2019. IEEE, 2001.
- [38] Shahir Hasanzadeh and Farrokh Janabi-Sharifi. Model-based force estimation for intracardiac catheters. *IEEE/ASME Transactions on Mechatronics*, 21(1):154–162, 2015.
- [39] Ian A Gravagne, Christopher D Rahn, and Ian D Walker. Large deflection dynamics and control for planar continuum robots. *IEEE/ASME transactions on mechatronics*, 8(2):299–307, 2003.
- [40] Bryan A Jones and Ian D Walker. Kinematics for multisection continuum robots. *IEEE Transactions on Robotics*, 22(1):43–55, 2006.
- [41] Mahta Khoshnam, Mahdi Azizian, and Rajni V Patel. Modeling of a steerable catheter based on beam theory. In *2012 IEEE International Conference on Robotics and Automation*, pages 4681–4686. IEEE, 2012.

- [42] MK Konings, EB Van de Kraats, T Alderliesten, and WJ Niessen. Analytical guide wire motion algorithm for simulation of endovascular interventions. *Medical and Biological Engineering and Computing*, 41(6):689–700, 2003.
- [43] Tim McInerney and Demetri Terzopoulos. Deformable models in medical image analysis. In *Proceedings of the workshop on mathematical methods in biomedical image analysis*, pages 171–180. IEEE, 1996.
- [44] Vincent Luboz, Jianhua Zhai, Tolu Odetoyinbo, Peter Littler, Derek Gould, Thien How, and Fernando Bello. Simulation of endovascular guidewire behaviour and experimental validation. *Computer methods in biomechanics and biomedical engineering*, 14(06):515–520, 2011.
- [45] Mohammad Jolaei, Amir Hooshier, and Javad Dargahi. Displacement-based model for estimation of contact force between rfa catheter and atrial tissue with ex-vivo validation. In *2019 IEEE International Symposium on Robotic and Sensors Environments (ROSE)*, pages 1–7. IEEE, 2019.
- [46] Amir Hooshier, Masoud Razban, Naghmeh M Bandari, and Javad Dargahi. Sensing principle for real-time characterization of viscoelasticity in the beating myocardial tissue. In *2017 IEEE International Conference on Computational Intelligence and Virtual Environments for Measurement Systems and Applications (CIVEMSA)*, pages 72–77. IEEE, 2017.
- [47] Ahmed A Shabana. Flexible multibody dynamics: review of past and recent developments. *Multibody system dynamics*, 1(2):189–222, 1997.
- [48] Julien Lenoir, Stephane Cotin, Christian Duriez, and Paul Neumann. Interactive physically-based simulation of catheter and guidewire. *Computers & Graphics*, 30(3):416–422, 2006.
- [49] Shuxiang Guo, Mingyang Qin, Nan Xiao, Yuan Wang, Weili Peng, and Xianqiang Bao. High precise haptic device for the robotic catheter navigation system. In *2016 IEEE International Conference on Mechatronics and Automation*, pages 2524–2529. IEEE, 2016.
- [50] Stéphane Cotin, Christian Duriez, Julien Lenoir, Paul Neumann, and Steven Dawson. New approaches to catheter navigation for interventional radiology simulation. In *International Conference on Medical Image Computing and Computer-Assisted Intervention*, pages 534–542. Springer, 2005.
- [51] RE Valembois, Paul Fiset, and Jean-Claude Samin. Comparison of various techniques for modelling flexible beams in multibody dynamics. *Nonlinear Dynamics*, 12(4):367–397, 1997.
- [52] Pier Paolo Valentini and Ettore Pennestrì. Modeling elastic beams using dynamic splines. *Multibody system dynamics*, 25(3):271–284, 2011.

- [53] Fernando M Cardoso and Sergio S Furuie. Guidewire path determination for intravascular applications. *Computer methods in biomechanics and biomedical engineering*, 19(6):628–638, 2016.
- [54] Wen Tang, Tao Ruan Wan, Derek A Gould, Thien How, and Nigel W John. A stable and real-time nonlinear elastic approach to simulating guidewire and catheter insertions based on cosserat rod. *IEEE Transactions on Biomedical Engineering*, 59(8):2211–2218, 2012.
- [55] Hugh Calkins, Karl Heinz Kuck, Riccardo Cappato, Josep Brugada, A John Camm, Shih-Ann Chen, Harry JG Crijns, Ralph J Damiano Jr, D Wyn Davies, John Di-Marco, et al. 2012 hrs/ehra/ecas expert consensus statement on catheter and surgical ablation of atrial fibrillation. *Europace*, 14(4):528–606, 2012.
- [56] Mohammad Jolaei, Amir Hooshier, Amir Sayadi, Javad Dargahi, and Muthukumar Packirisamy. Sensor-free force control of tendon-driven ablation catheters through position control and contact modeling. In *2020 42nd Annual International Conference of the IEEE Engineering in Medicine & Biology Society (EMBC)*, pages 5248–5251. IEEE, 2020.
- [57] Mark Runciman, Ara Darzi, and George P Mylonas. Soft robotics in minimally invasive surgery. *Soft robotics*, 6(4):423–443, 2019.
- [58] Faisal Hasan and Johannes Bonatti. Robotically assisted percutaneous coronary intervention: benefits to the patient and the cardiologist, 2015.
- [59] Mahta Khoshnam, Aaron Yurkewich, and Rajni V Patel. Model-based force control of a steerable ablation catheter with a custom-designed strain sensor. In *2013 IEEE International Conference on Robotics and Automation*, pages 4479–4484. IEEE, 2013.
- [60] Angelica I Aviles, Samar M Alsaleh, James K Hahn, and Alicia Casals. Towards retrieving force feedback in robotic-assisted surgery: A supervised neuro-recurrent-vision approach. *IEEE transactions on haptics*, 10(3):431–443, 2016.
- [61] Masoud Kalantari, Mohammadreza Ramezanifard, Roozbeh Ahmadi, Javad Dargahi, and József Kövecses. A piezoresistive tactile sensor for tissue characterization during catheter-based cardiac surgery. *The International Journal of Medical Robotics and Computer Assisted Surgery*, 7(4):431–440, 2011.
- [62] János Radó, Csaba Dücső, Péter Földesy, Gábor Szabó, Zbigniew Nawrat, Kamil Rohr, and Péter Fürjes. 3d force sensors for laparoscopic surgery tool. *Microsystem Technologies*, 24(1):519–525, 2018.
- [63] Panagiotis Polygerinos, Tobias Schaeffter, Lakmal Seneviratne, and Kaspar Althofer. A fibre-optic catheter-tip force sensor with mri compatibility: A feasibility study. In *2009 Annual International Conference of the IEEE Engineering in Medicine and Biology Society*, pages 1501–1054. IEEE, 2009.

- [64] Santhi Elayaperumal, Jung Hwa Bae, Bruce L Daniel, and Mark R Cutkosky. Detection of membrane puncture with haptic feedback using a tip-force sensing needle. In *2014 IEEE/RSJ International Conference on Intelligent Robots and Systems*, pages 3975–3981. IEEE, 2014.
- [65] Lei Zhang, Feng Ju, Yanfei Cao, Yaoyao Wang, and Bai Chen. A tactile sensor for measuring hardness of soft tissue with applications to minimally invasive surgery. *Sensors and Actuators A: Physical*, 266:197–204, 2017.
- [66] Junwoo Lee, Wook Choi, Yong Kyoung Yoo, Kyo Seon Hwang, Sang-Myung Lee, Sungchul Kang, Jinseok Kim, and Jeong Hoon Lee. A micro-fabricated force sensor using an all thin film piezoelectric active sensor. *Sensors*, 14(12):22199–22207, 2014.
- [67] Ali Talasaz and Rajni V Patel. Integration of force reflection with tactile sensing for minimally invasive robotics-assisted tumor localization. *IEEE Transactions on Haptics*, 6(2):217–228, 2012.
- [68] Uikyum Kim, Yong Bum Kim, Dong-Yeop Seok, and Hyouk Ryeol Choi. S-surge: A portable surgical robot based on a novel mechanism with force-sensing capability for robotic surgery. In *Handbook of Robotic and Image-Guided Surgery*, pages 265–283. Elsevier, 2020.
- [69] Bruno Gil, Bing Li, Anzhu Gao, and Guang-Zhong Yang. Miniaturized piezo force sensor for a medical catheter and implantable device. *ACS applied electronic materials*, 2(8):2669–2677, 2020.
- [70] Mahta Khoshnam and Rajni V Patel. Estimating contact force for steerable ablation catheters based on shape analysis. In *2014 IEEE/RSJ International Conference on Intelligent Robots and Systems*, pages 3509–3514. IEEE, 2014.
- [71] Mahta Khoshnam, Allan C Skanes, and Rajni V Patel. Modeling and estimation of tip contact force for steerable ablation catheters. *IEEE Transactions on Biomedical Engineering*, 62(5):1404–1415, 2015.
- [72] Linshuai Zhang, Shuxiang Guo, Huadong Yu, and Yu Song. Performance evaluation of a strain-gauge force sensor for a haptic robot-assisted catheter operating system. *Microsystem Technologies*, 23(10):5041–5050, 2017.
- [73] Hoseok Song, Heechul Kim, Juwon Jeong, and Jungju Lee. Development of fbg sensor system for force-feedback in minimally invasive robotic surgery. In *2011 Fifth International Conference on Sensing Technology*, pages 16–20. IEEE, 2011.
- [74] Abdulrahman Albakri. *Haptic Teleoperation for Robotic-Assisted Surgery*. PhD thesis, Université Montpellier, 2015.
- [75] Vincent Hayward and Karon E MacLean. Do it yourself haptics: part i. *IEEE Robotics & Automation Magazine*, 14(4):88–104, 2007.

- [76] Domenico Prattichizzo, Jeffrey C Trinkle, Bruno Siciliano, and Oussama Khatib. Springer handbook of robotics. *Grasping; Springer: Berlin/Heidelberg, Germany*, pages 671–700, 2008.
- [77] Amir Hooshiar, Naghmeh Bandari, and Javad Dargahi. Image-based estimation of contact forces on catheters for robot-assisted cardiovascular intervention. In *Hamlyn Symposium on Medical Robotics*, pages 119–120, 2018.
- [78] Prapa Kanagaratnam, Michael Koa-Wing, Daniel T Wallace, Alex S Goldenberg, Nicholas S Peters, and D Wyn Davies. Experience of robotic catheter ablation in humans using a novel remotely steerable catheter sheath. *Journal of Interventional Cardiac Electrophysiology*, 21(1):19–26, 2008.
- [79] Chad M Dugas and Jeffrey M Schussler. Advanced technology in interventional cardiology: a roadmap for the future of precision coronary interventions. *Trends in cardiovascular medicine*, 26(5):466–473, 2016.
- [80] Arnold H Seto and Morton J Kern. Robotic-assist pci: Precision guided pci or a rube goldberg solution?, 2014.
- [81] Kamran Ahmed, Aoife N Keeling, Morkos Fakhry, Hutan Ashrafian, Rajesh Aggarwal, Peter A Naughton, Ara Darzi, Nicholas Cheshire, Thanos Athanasiou, and Mohammed Hamady. Role of virtual reality simulation in teaching and assessing technical skills in endovascular intervention. *Journal of Vascular and Interventional Radiology*, 21(1):55–66, 2010.
- [82] Hedyeh Rafii-Tari, Christopher J Payne, and Guang-Zhong Yang. Current and emerging robot-assisted endovascular catheterization technologies: a review. *Annals of biomedical engineering*, 42(4):697–715, 2014.
- [83] Christopher J Payne, Hedyeh Rafii-Tari, and Guang-Zhong Yang. A force feedback system for endovascular catheterisation. In *2012 IEEE/RSJ International Conference on Intelligent Robots and Systems*, pages 1298–1304. IEEE, 2012.
- [84] Jagadeesan Jayender, Rajnikant V Patel, and Suwas Nikumb. Robot-assisted active catheter insertion: Algorithms and experiments. *The International Journal of Robotics Research*, 28(9):1101–1117, 2009.
- [85] YingLiang Ma, Graeme P Penney, Dennis Bos, Peter Frissen, C Aldo Rinaldi, Reza Razavi, and Kawal S Rhode. Hybrid echo and x-ray image guidance for cardiac catheterization procedures by using a robotic arm: a feasibility study. *Physics in Medicine & Biology*, 55(13):N371, 2010.
- [86] Giulio Dagnino, Jindong Liu, Mohamed EMK Abdelaziz, Wenqiang Chi, C Riga, and G-Z Yang. Haptic feedback and dynamic active constraints for robot-assisted endovascular catheterization. In *2018 IEEE/RSJ International Conference on Intelligent Robots and Systems (IROS)*, pages 1770–1775. IEEE, 2018.

- [87] Xuanchun Yin, Shuxiang Guo, Nan Xiao, Takashi Tamiya, Hideyuki Hirata, and Hi-denori Ishihara. Safety operation consciousness realization of a mr fluids-based novel haptic interface for teleoperated catheter minimally invasive neurosurgery. *IEEE/ASME Transactions on Mechatronics*, 21(2):1043–1054, 2015.
- [88] Linshuai Zhang, Shuxiang Guo, Huadong Yu, Shuoxin Gu, Yu Song, and Miao Yu. Electromagnetic braking-based collision protection of a novel catheter manipulator. In *2017 IEEE International Conference on Mechatronics and Automation (ICMA)*, pages 1726–1731. IEEE, 2017.
- [89] Xuanchun Yin, Shuxiang Guo, and Yu Song. Magnetorheological fluids actuated haptic-based teleoperated catheter operating system. *Micromachines*, 9(9):465, 2018.
- [90] Amir Sayadi, Amir Hooshair, and Javad Dargahi. Impedance matching approach for robust force feedback rendering with application in robot-assisted interventions. In *2020 8th International Conference on Control, Mechatronics and Automation (ICCMA)*, pages 18–22. IEEE, 2020.
- [91] Amir Hooshair, Amir Sayadi, Javad Dargahi, and Siamak Najarian. Integral-free spatial orientation estimation method and wearable rotation measurement device for robot-assisted catheter intervention. *IEEE/ASME Transactions on Mechatronics*, 2021.
- [92] Hooshair Amir, Amir Sayadi, Mohammad Jolaei, and Javad Dargahi. Analytical tip force estimation on tendon-driven catheters through inverse solution of cosserat rod model. In *2021 International Conference on Intelligent Robotic Systems (IROS)*. IEEE, 2021.
- [93] Amir Hooshair, Amir Sayadi, Mohammad Jolaei, and Javad Dargahi. Accurate estimation of tip force on tendon-driven catheters using inverse cosserat rod model. In *2020 International Conference on Biomedical Innovations and Applications (BIA)*, pages 37–40. IEEE, 2020.
- [94] Naghmeh M Bandari, Roozbeh Ahmadi, Amir Hooshair, Javad Dargahi, and Muthukumaran Packirisamy. Hybrid piezoresistive-optical tactile sensor for simultaneous measurement of tissue stiffness and detection of tissue discontinuity in robot-assisted minimally invasive surgery. *Journal of biomedical optics*, 22(7):077002, 2017.
- [95] Naghmeh M Bandari, Amir Hooshair, Muthukumaran Packirisamy, and Javad Dargahi. Optical fiber array sensor for lateral and circumferential force measurement suitable for minimally invasive surgery: Design, modeling and analysis. In *Specialty Optical Fibers*, pages JTU4A–44. Optical Society of America, 2016.

- [96] Mohammad Jolaei, Amir Hooshier, Javad Dargahi, and Muthukumaran Packirisamy. Toward task autonomy in robotic cardiac ablation: Learning-based kinematic control of soft tendon-driven catheters. *Soft Robotics*, 2020.
- [97] Kazuto Takashima, Rei Shimomura, Takayuki Kitou, Hiroki Terada, Kiyoshi Yoshinaka, and Ken Ikeuchi. Contact and friction between catheter and blood vessel. *Tribology International*, 40(2):319–328, 2007.
- [98] A. Hooshier, A. Sayadi, M. Jolaei, and J. Dargahi. Accurate estimation of tip force on tendon-driven catheters using inverse cosserat rod model. In *2020 IEEE International Conference on Biomedical innovations and Applications (BIA)*, volume *Inpress*. IEEE, 2020.
- [99] Pegah Yaftian, Naghmeh Bandari, Amir Hooshier, and Javad Dargahi. Image-based contact detection and static force estimation on steerable rfa catheters. In *2020 International Conference on Biomedical Innovations and Applications (BIA)*, pages 57–60. IEEE, 2020.
- [100] Edsger W Dijkstra. A note on two problems in connexion with graphs. *Numerische mathematik*, 1(1):269–271, 1959.
- [101] Rida T Farouki. *Pythagorean—hodograph Curves*. Springer, 2008.
- [102] Amir Hooshier, Alireza Payami, Javad Dargahi, and Siamak Najarian. Magnetostriction-based force feedback for robot-assisted cardiovascular surgery using smart magnetorheological elastomers. *Mechanical Systems and Signal Processing*, 161:107918, 2021.
- [103] Mohammad Jolaei, Amir Hooshier, Javad Dargahi, and Muthukumaran Packirisamy. Toward task autonomy in robotic cardiac ablation: Learning-based kinematic control of soft tendon-driven catheters. *Soft Robotics*, Accepted(2020.0006), 2020.
- [104] Maya S Verma, Maria Terricabras, and Atul Verma. The cutting edge of atrial fibrillation ablation. *Arrhythmia & Electrophysiology Review*, 10(2):101, 2021.
- [105] A. Hooshier, S. Najarian, and J. Dargahi. Haptic telerobotic cardiovascular intervention: A review of approaches, methods, and future perspectives. *IEEE Reviews in Biomedical Engineering*, 13:32–50, 2020.
- [106] Tejas M Patel, Sanjay C Shah, and Samir B Pancholy. Long distance tele-robotic-assisted percutaneous coronary intervention: a report of first-in-human experience. *EClinicalMedicine*, 14:53–58, 2019.
- [107] Mohammad Dado and Samir Al-Sadder. A new technique for large deflection analysis of non-prismatic cantilever beams. *Mechanics research communications*, 32(6):692–703, 2005.

- [108] Kyungwoo Lee. Post-buckling of uniform cantilever column under a combined load. *International Journal of Non-Linear Mechanics*, 36(5):813–816, 2001.
- [109] Anders Magnusson, Matti Ristinmaa, and Christer Ljung. Behaviour of the extensible elastica solution. *International Journal of Solids and Structures*, 38(46-47):8441–8457, 2001.
- [110] Taoming Liu, Nate Lombard Poirot, Dominique Franson, Nicole Seiberlich, Mark A Griswold, and M Cenk Çavuşoğlu. Modeling and validation of the three-dimensional deflection of an mri-compatible magnetically actuated steerable catheter. *IEEE Transactions on Biomedical Engineering*, 63(10):2142–2154, 2015.
- [111] BW Kooi and M Kuipers. A unilateral contact problem with the heavy elastica. *International journal of non-linear mechanics*, 19(4):309–321, 1984.
- [112] BW Golley. The solution of open and closed elasticas using intrinsic coordinate finite elements. *Computer methods in applied mechanics and engineering*, 146(1-2):127–134, 1997.
- [113] Jonas Spillmann and Matthias Teschner. Corde: Cosserat rod elements for the dynamic simulation of one-dimensional elastic objects. In *Proceedings of the 2007 ACM SIGGRAPH/Eurographics symposium on Computer animation*, pages 63–72, 2007.
- [114] Ilker Tunay. Spatial continuum models of rods undergoing large deformation and inflation. *IEEE Transactions on Robotics*, 29(2):297–307, 2013.
- [115] Farrokh Janabi-Sharifi, Amir Jalali, and Ian D Walker. Cosserat rod-based dynamic modeling of tendon-driven continuum robots: A tutorial. *IEEE Access*, 9:68703–68719, 2021.
- [116] SM Hadi Sadati, Ali Shiva, Nicolas Herzig, Caleb D Rucker, Helmut Hauser, Ian D Walker, Christos Bergeles, Kaspar Althoefer, and Thrishantha Nanayakkara. Stiffness imaging with a continuum appendage: real-time shape and tip force estimation from base load readings. *IEEE Robotics and Automation Letters*, 5(2):2824–2831, 2020.
- [117] Vincent Aloï and Caleb Rucker. Estimating loads along elastic rods. In *2019 International Conference on Robotics and Automation (ICRA)*, pages 2867–2873, May 2019.
- [118] Majid Roshanfar, Javad Dargahi, and Amir Hooshair. Toward semi-autonomous stiffness adaptation of pneumatic soft robots: Modeling and validation. In *2021 International Conference on Autonomous Systems*. IEEE, 2021.
- [119] Naghmeh M Bandari, Amir Hooshair, Packirisamy Muthukumaran, and Javad Dargahi. Bending-based formulation of light intensity modulation for miniaturization

- of optical tactile sensors. In *Optical Sensors*, pages SeM2E–3. Optical Society of America, 2018.
- [120] N. Bandari, J. Dargahi, and M. Packirisamy. Tactile sensors for minimally invasive surgery: A review of the state-of-the-art, applications, and perspectives. *IEEE Access*, 8:7682–7708, 2020.
- [121] Amir Hooshier, Ali Alkhalaf, and Javad Dargahi. Development and assessment of a stiffness display system for minimally invasive surgery based on smart magneto-rheological elastomers. *Materials Science and Engineering: C*, 108:110409, 2020.
- [122] Ryan D Madder, Stacie VanOosterhout, Jessica Parker, Kalyna Sconzert, Yao Li, Nicholas Kottenstette, Abigail Madsen, John-Michael Sungur, and Per Bergman. Robotic telestenting performance in transcontinental and regional pre-clinical models. *Catheterization and Cardiovascular Interventions*, 2020.
- [123] Meryem Simsek, Adnan Aijaz, Mischa Dohler, Joachim Sachs, and Gerhard Fettweis. 5g-enabled tactile internet. *IEEE Journal on Selected Areas in Communications*, 34(3):460–473, 2016.
- [124] Yuan Wang, Shuxiang Guo, Nan Xiao, Youxiang Li, and Yuhua Jiang. Online measuring and evaluation of guidewire inserting resistance for robotic interventional surgery systems. *Microsystem Technologies*, pages 1–11, 2018.
- [125] Shuxiang Guo, Yu Song, Xuanchun Yin, Linshuai Zhang, Takashi Tamiya, Hideyuki Hirata, and Hidenori Ishihara. A novel robot-assisted endovascular catheterization system with haptic force feedback. *IEEE Transactions on Robotics*, 35(3):685–696, 2019.
- [126] Mojtaba Sharifi, Hassan Salarieh, Saeed Behzadipour, and Mahdi Tavakoli. Beating-heart robotic surgery using bilateral impedance control: Theory and experiments. *Biomedical signal processing and control*, 45:256–266, 2018.